Diagenesis, compaction strain and deformation associated with chert and carbonate concretions in organic-rich marl and phosphorite; Upper Cretaceous to Eocene, Jordan

ISRAA S. ABU-MAHFOUZ* iD , JOE A. CARTWRIGHT†, JOHN H. POWELL‡, MOHAMMAD S. ABU-MAHFOUZ§ and OLAF G. PODLAHA¶
*Department of Geosciences, College of Petroleum Engineering & Geosciences (CPG), King Fahd University of Petroleum & Minerals (KFUPM), Dhahran, 31261, Saudi Arabia (E-mail: israa.abumahfouz@kfupm.edu.sa)
†Department of Earth Sciences, University of Oxford, South Parks Road, Oxford, OX1 3AN, UK
‡British Geological Survey, Nicker Hill, Keyworth, Nottingham, NG12 5GG, UK
§School of Health and Education, Middlesex University, The Burroughs, London, NW4 4BT, UK
¶Shell Global Solutions International B.V., Projects and Technology, Rijswijk, 2288 ER, The Netherlands

ABSTRACT

This paper presents an integrated petrographic–geochemical–geomechanical study of the growth mechanisms of carbonate and chert concretions observed at outcrop and core from the Upper Cretaceous to Eocene organic-rich carbonate mudrocks, central Jordan. It provides evidence for displacive and replacive concretion growth from the analysis of primary lithological characteristics, compaction strain and deformation structures associated with concretion growth. Concretions were analysed to determine the primary lithological controls on their development and the measurement of strain in the host rock to develop a method for constraining the growth mode and their paragenesis. Concretions exhibit either a replacive or displacive growth mode largely dependent on the original host lithology. Displacive concretions exhibit irregular shapes and semi-fibrous internal structures in contrast to regular shapes and microcrystalline textures observed for replacive concretions. Cement fraction is high in both carbonate concretion types, indicating early formation in high-porosity sediments at shallow burial depths. The strain field around displacive concretions is vertically asymmetrical. Conversely, it is symmetrical with uniform differential compaction for the replacive concretions. Evidence for displacive growth comes from triangular areas of chert at the lateral margins of some carbonate concretions, interpreted as areas of reduced strain. Another indicator is the forced asymmetrical folding of heterolithic host rocks around displacive concretions, with displacive carbonate units separated by trace laminae of the original (chert) beds. Enveloping chert beds exhibit early-formed radial silica fractures with increased aperture size in the areas of maximum curvature. Carbon isotopic signatures of carbonate concretions show a strong correlation between concretion centres and host rock, suggesting a relatively shallow depth (first few tens of metres) of initial growth. Carbonate concretions are interpreted to have formed at shallow depths in the presence of alkaline pore waters rich in dissolved organic carbon in the presence of Mg^{2+} ions, available organic matter and redox-sensitive metals such as U and Mo. A paragenetic history for the different concretion types is presented.

INTRODUCTION

The occurrence of concretions in mudrocks is a typical diagenetic characteristic of the host rock formation (Astin & Scotchman, 1988) that strongly reflects the primary sediment compositions and pore water chemistry (Raiswell, 1971, 1976, 1988; Huggett, 1994; Sellés-Martinez, 1996; Hesse & Schacht, 2011; Dale et al., 2014; Gaines & Vorhies, 2016). Concretion composition varies from dominantly carbonate minerals to micro-crystalline quartz, most commonly with single dominant mineralogy for individual concretions (i.e. carbonate concretions or silica concretions). More rarely, concretions with concentric zones of carbonate and silica (Raiswell, 1971; Nelson & Lawrence, 1984), clay concretions (for example, kaolinite) and pyrite nodules/concretions (e.g. Emmings et al., 2020) are also recorded. In addition, pyrite often rims or is enriched in concentric layers within carbonate and chert concretions (e.g. Xiao et al., 2010). Gypsum, baryte and phosphate concretions are also important in some fine-grained sediments because they can help to constrain the paragenetic model (Emmings et al., 2020). Compositional differences in concretions have been attributed to the variation in the diagenetic environment during concretion formation, which is controlled by the composition of the host rock (sediment) and depositional environment (Woo & Khim, 2006). The nature of the concretion cement, texture and porosity can help to constrain the mode and depth of the concretion growth (Raiswell, 1971).

The majority of concretions are documented in mudstones (e.g. Dix & Mullins, 1987; Astin & Scotchman, 1988; Hesslebo & Palmer, 1992; Huggett, 1994; Mozley, 1996; Raiswell & Fisher, 2000; Raiswell et al., 2002; Pearson & Nelson, 2005; Marshall & Pirrie, 2013; Gaines & Vorhies, 2016). However, some of the examples described here are present in heterolithic phosphorite strata (chalky marl–chert–phosphate lithofacies). Concretions can be associated with natural fractures, which makes them of potential interest to resource evaluation wherever natural fractures in shales or mudrocks are relevant (for example, petroleum seal analysis, shale gas exploitation). In some cases, fractures are self-contained (for example, septarian fractures; Astin, 1986), truncate (for example, bitumen-filled fractures; Abu-Mahfouz et al., 2020) or develop immediately adjacent to the concretions in different geometrical arrays (Rodrigues et al., 2009; Hooker et al., 2017, 2019; Meng et al., 2018; Abu-Mahfouz, 2019).

Concretions commonly exhibit one mode of growth that reveals its formation mechanism (e.g. Raiswell, 1971; Sellés-Martinez, 1996; Pearson & Nelson, 2005; Woo & Khim, 2006; Marshall & Pirrie, 2013). However, a few studies have reported two modes of growth in the same concretion body, which usually occur as alternating zones (e.g. Gaines & Vorhies, 2016; Liu et al., 2019).

Identifying the mechanism(s) that control concretion growth is commonly problematic (Raiswell & Fisher, 2000), but growth mode can be constrained by integrated petrographic, geochemical and geomechanical investigations, the main aim of this study. Examining the changes in the competency, pore pressure and diagenetic pathways in the surrounding rock from one layer to another contributes to our understanding of concretion growth. The abundance of carbonate and chert concretions in the Upper Cretaceous–Eocene strata of Jordan, known as the Jordan Oil Shale (JOS), offers an opportunity to examine the different modes of concretion growth in a variety of host rock lithologies. Another aim of this study is to place the mode of concretion growth in a stratigraphical context, and relate this to the diagenetic and burial history of the host rocks. The relative timing of concretion growth was constrained in this study by an analysis of the amount of compaction in the concretion by comparison with the adjacent host rocks (cf. Craig, 1985; Astin & Scotchman, 1988) and an interpretation of relative stages of lithification at, or below, the sediment–water interface. This extends a previous attempt to quantify differential compaction around concretions by Hooker et al. (2017) and integrates the findings of this strain analysis with the sedimentological and petrographical observations.

METHODOLOGY

Sample selection

Observations of concretions in the 'Jordan Oil Shales' (JOS) were conducted at outcrops and in cores. Field observations focused on a contextual study of the distribution of different types of concretions, and their association with varied host-rock lithologies and associated fractures. Concretions were sampled from outcrop and core for petrographic and geochemical analysis. Subsamples were systematically selected from the centre to edge of concretions from each individual concretion horizon. Fifteen cores (C1–

C15) that intersected the JOS from central Jordan were described, logged and sampled (Fig. 1A). Five key outcrop locations in central and south Jordan were logged and sampled; Harrana, El-Lajjun, Qatrana, Sultani and Wadi Al-Bustani (Fig. 1A and B; Fig. S1; Table S1).

Methods

Geochemical and petrographical investigations were conducted on selected samples in order to understand the growth mechanisms of the concretions. Concretions were recorded in the field and in the core with the aid of digital photographs. Stable isotope analyses of the bulk
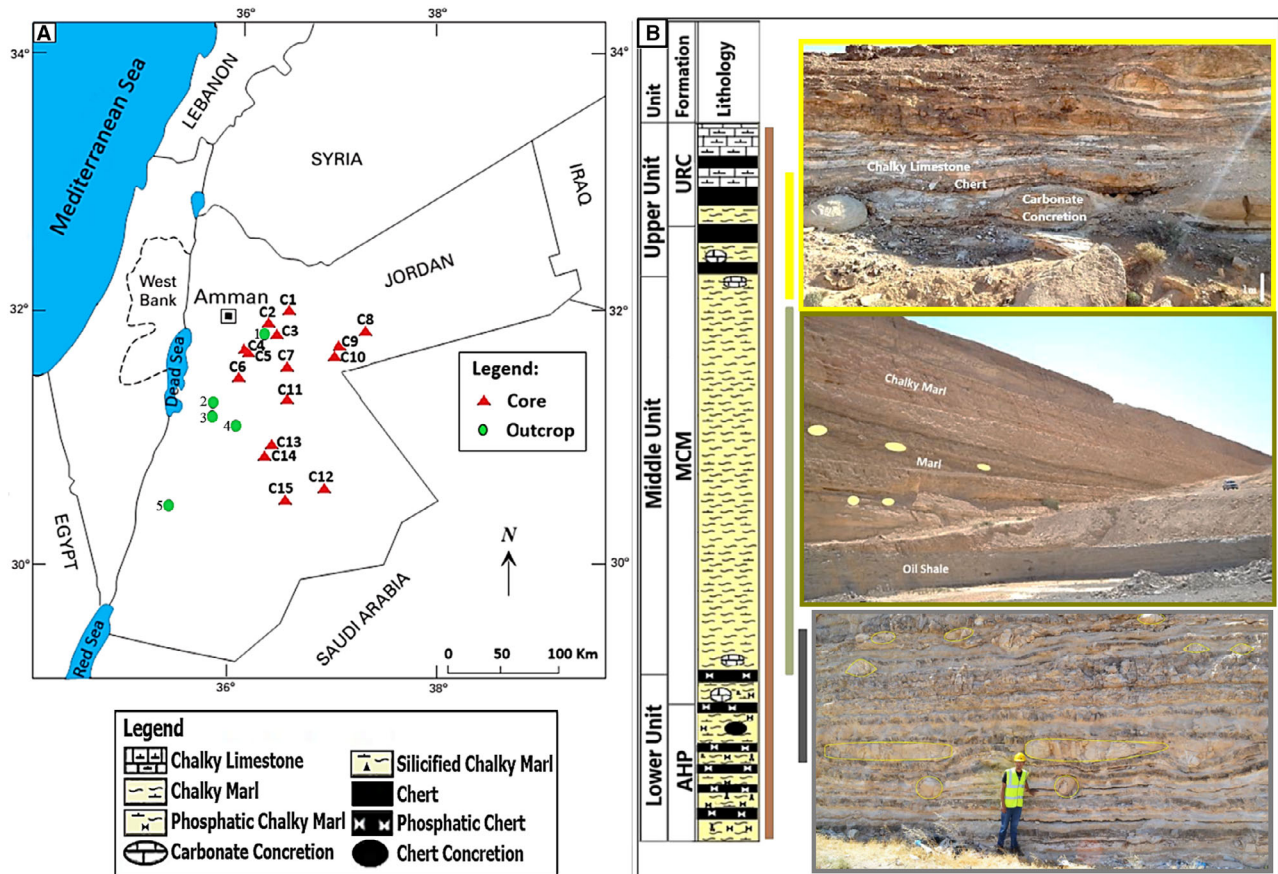

Fig. 1. (A) Map of Jordan showing the location of the study cores (red triangles) and outcrops (green circles; 1: Harrana outcrop, 2: El-Lajjun quarry, 3: Qatrana Roadcut; 4: Sultani Quarry, 5: Wadi Al-Bustani outcrop). (B) A schematic columnar section showing the lithology of the studied succession. Note the distribution of the chert and carbonate concretions. On the right, a representation of the study succession from the different study outcrops. Brown line represents the whole succession in Wadi Al-Bustani; grey line represents the Qatrana Roadcut; green line represents the Sultani and El-Lajjun Quarries; yellow line represents the Harrana Outcrop. Grey-framed photograph from the Qatrana Roadcut; green-framed photograph from the Sultani Quarry; yellow-framed photograph from the Harrana Outcrop. Note the different concretion horizons (beige ellipsoids and circles). Note that specific concretion morphologies are restricted to specific concretion layers. Person for scale is *ca* 1.8 m tall.

carbon $\delta^{13}C$ and oxygen $\delta^{18}O$ from calcite were conducted on systematically selected subsamples (centre to edge) from carbonate concretions using a MAT-253 mass spectrometer (Thermo Fisher Scientific, Waltham, MA, USA). Before conducting the analysis, the powdered samples were cleaned using hydrogen peroxide (H_2O_2) and dried in the oven at 40°C. Concentrated phosphoric acid (H_3PO_4) was added to the samples to produce the CO_2 for analysis.

Petrographic study was performed on thin sections prepared from samples taken from carbonate/chert concretions and their host rocks using cross-polarized light under a Nikon-Optophot Microscope (Nikon, Tokyo, Japan) linked to a high-resolution digital camera. Selected samples of concretions and host rocks were investigated under an FEI-Quanta-650-FEG Scanning Electron Microscope (SEM; FEI Quanta, Hillsboro, OR, USA) at a working distance of 10 mm. Backscattered scanning electron microscopy (BSE) images were generated to study the mineral compositions and textures of samples. Elemental mapping was performed using an energy dispersive spectrometer (EDS) attached to the SEM.

GEOLOGICAL FRAMEWORK

Jordan is situated at the north-western margin of the Arabian Plate. The Upper Cretaceous–Eocene succession, which includes organic-rich phosphorite and bituminous chalky marls, is also informally known as the Jordan Oil Shale (Alqudah *et al.*, 2015). It represents a passive continental margin sequence deposited on a shallow-water pelagic–hemi-pelagic ramp succession (Belqa Group) that was initiated in Coniacian times in marked contrast to the underlying Cenomanian to Turonian rimmed carbonate shelf (Ajlun Group) (Powell & Moh'd, 2011). During Maastrichtian to Eocene times, progressive south-eastward onlap of Neo-Tethys resulted in increasingly deeper water, pelagic sedimentation influenced by oceanic upwelling that resulted in the deposition of phosphorite and organic-rich calcareous mudstones. Structures and sedimentation were greatly influenced by syndepositional and post-depositional tectonics (Abu-Jaber *et al.*, 1989). Hence, the Upper Cretaceous–Lower Eocene organic-rich carbonate mudrocks of Jordan were deposited in local, isolated depocentres on the carbonate platform (Powell & Moh'd, 2011). The area experienced

rift flank uplift in the later Neogene during the establishment of the Dead-Sea Rift System (Feinstein *et al.*, 2013). This uplift led to an eastward tilt from the outcropping rim of JOS at the Dead Sea escarpment, to reach maximum present-day burial depths of just over 1000 m in eastern Jordan, part of the Arabian Platform. Representative burial history curves can be found in Abu-Mahfouz *et al.* (2019).

In the central Jordan study area, the structure is mainly controlled by normal, high-angle faults trending NNW–SSE, and for the most part concave to the north-east. Block faulting along curved faults with opposing downthrows led to the formation of the Sultani depression, a north-west/south-east trending graben structure. The main structural feature in the El-Lajjun area is the El-Lajjoun Graben, which controls a topographical depression surrounded to the East and West by north–south striking faults (Shawabkeh, 1991).

The study interval (JOS) comprises three formations (upper Belqa Group) in an upward sequence: Al-Hisa Phosphorite Formation (AHP), Muwaqqar Chalk Marl Formation (MCM); and Umm Rijam Chert Limestone Formation (URC) (Fig. 1B, Table S1; Powell, 1989), exposed at the outcrop. The heterolithic AHP consists mainly of phosphorite comprising granular phosphate, phosphatic chert, shelly limestone, chalky marl, porcellanite and bituminous marl. This formation contains abundant bivalves (including oysters), fish/reptile fragments and foraminifera suggesting a shallow-water pelagic depositional environment (Powell & Moh'd, 2011; Grohmann *et al.*, 2023). Chert and carbonate concretions are abundant in the AHP. The overlying MCM comprises interbedded bituminous marl (oil shale), thin phosphatic limestone, marly limestone and chert beds with abundant concretions in the lower part, homogenous chalky and bituminous marl in the middle part, and yellowish marl, chalky marl and black chert in the upper part. The URC is composed of alternating beds of chalky limestones, chalky marl, marly limestones, limestones, and abundant chert beds and concretions. Carbonate concretions and burrowed 'firm grounds' are abundant at the MCM/URC boundary (Fig. 1B). Shell fragments, fish teeth and bones, and microfossils (calcareous nanoplankton and foraminifera) are present in this formation. These lithofacies and biofacies indicate a deepwater environment of deposition for the URC (Powell & Moh'd, 2011; Alqudah *et al.*, 2015; Grohmann *et al.*, 2023).

Discontinuous outcrops in central Jordan, expose the major part of the study succession (Fig. 1B), while the outcrop in Wadi Al-Bustani (south Jordan) exposes the entire succession (Fig. S1A). The present study subdivides the JOS study succession into three main units (Lower, Middle and Upper) (Fig. 1B) based on lithotypes and the presence (Lower and Upper units) or absence (Middle Unit) of chert beds/concretions. These informal units are broadly coincident with the formations outlined above.

Total organic carbon (TOC) values in these rocks range from 3 to 30% with increased TOC values in the lower part of the succession, the MCM (Alqudah *et al.*, 2015; Hakimi *et al.*, 2016; März *et al.*, 2016; Abu-Mahfouz *et al.*, 2019, 2020, 2022a, 2022b, 2023; Grohmann *et al.*, 2021, 2023). The rocks exhibit a complex diagenetic history (Powell & Moh'd, 2012; Hooker *et al.*, 2017; Huggett *et al.*, 2017), with an abundance of different diagenetic features (for example, chert beds, chert/carbonate concretions and early diagenetic folding). Huggett *et al.* (2017) linked the diagenesis in these organic-rich rocks to the fluctuating sedimentary environment of this shelf depositional system, and its influence on the composition of the deposited sediment and the early burial diagenetic environment. According to their study, most cementation is believed to have occurred early, generally within the first 10 m of burial (and entirely within the first 100 m of burial).

MACROSCOPIC CHARACTERIZATION OF CONCRETIONS

Composition and stratigraphical distribution

Four main compositional end members are observed: (i) carbonate concretions (Figs 2A, 2G, 3A and 3B); (ii) chert concretions (Fig. 2H and J); (iii) composite concretions composed of concentric zonation of carbonate and silica (Figs 2B, 2E, 2F, 2I and 3C); and (iv) 'winged' concretions with chert filling triangular areas at their lateral margins (Figs 2C, 2D, 3D and S2B). The composite concretions consist either of a chert concretion core enclosed by a carbonate zone (Fig. 2E, 2F and 2I) or of a carbonate concretion core surrounded by a chert zone (Fig. 2F).

Specific compositional types of concretions are restricted to specific concretion 'horizons',

that is, a single horizon has only one type (i.e. carbonate or chert) of concretion that is characterized by a specific morphology (Fig. 1B).

Carbonate and chert concretions are mainly clustered in distinct zones in the lower unit (for example, the Qatrana roadcut; AHP) and upper part of the study succession (the Harrana outcrop; URC; Fig. 1B). Carbonate concretions are occasionally observed in the middle part (MCM) (for example, El-Lajjun quarry) in the chalk marl layers. The full succession is exposed in Wadi Al-Bustani (Fig. S1A), where the distribution and orientation of the concretions were studied in a continuous section. This locality also afforded an exposure of concretions on an extensive bedding plane (Fig. S1B), allowing the planform distribution and morphology to be observed in detail.

Morphology and dimensions

A wide range of concretion morphologies is observed (Figs 2 and 3); these are defined as follows:

Type I-carbonate concretions (Type I-carb): Symmetrical, regular microcrystalline carbonate concretions, generally preserving original primary lamination, typically present in the MCM.

Type II-carbonate concretions (Type II-carb): Asymmetrical, irregular microcrystalline carbonate concretions, lacking primary lamination in the carbonate but may preserve traces of original chert laminae; they are typically present in the AHP (and rarely observed in the lower MCM). Type I-chert concretions (Type I-ch): Regular/irregular chert concretions that are usually associated with folded veins, typically present in AHP.

Type II-chert concretions (Type II-ch): Regular/ irregular chert concretions that are characterized by a transitional boundary with the surrounding sediments. They usually show a halo around them and are typically present in the AHP.

Some examples are observed to be symmetrical about a plane parallel to bedding (Figs 2A, 2G, 3A and 3B). Symmetrical concretions exhibit varied morphologies, including spherical, elliptical, tabular or lenticular, with different compositions. In the core, chert concretions in the AHP/lower MCM are commonly elliptical or lenticular and rarely irregular (Fig. 3H). Carbonate concretions in the core are commonly observed to be symmetrical, with spherical or elliptical
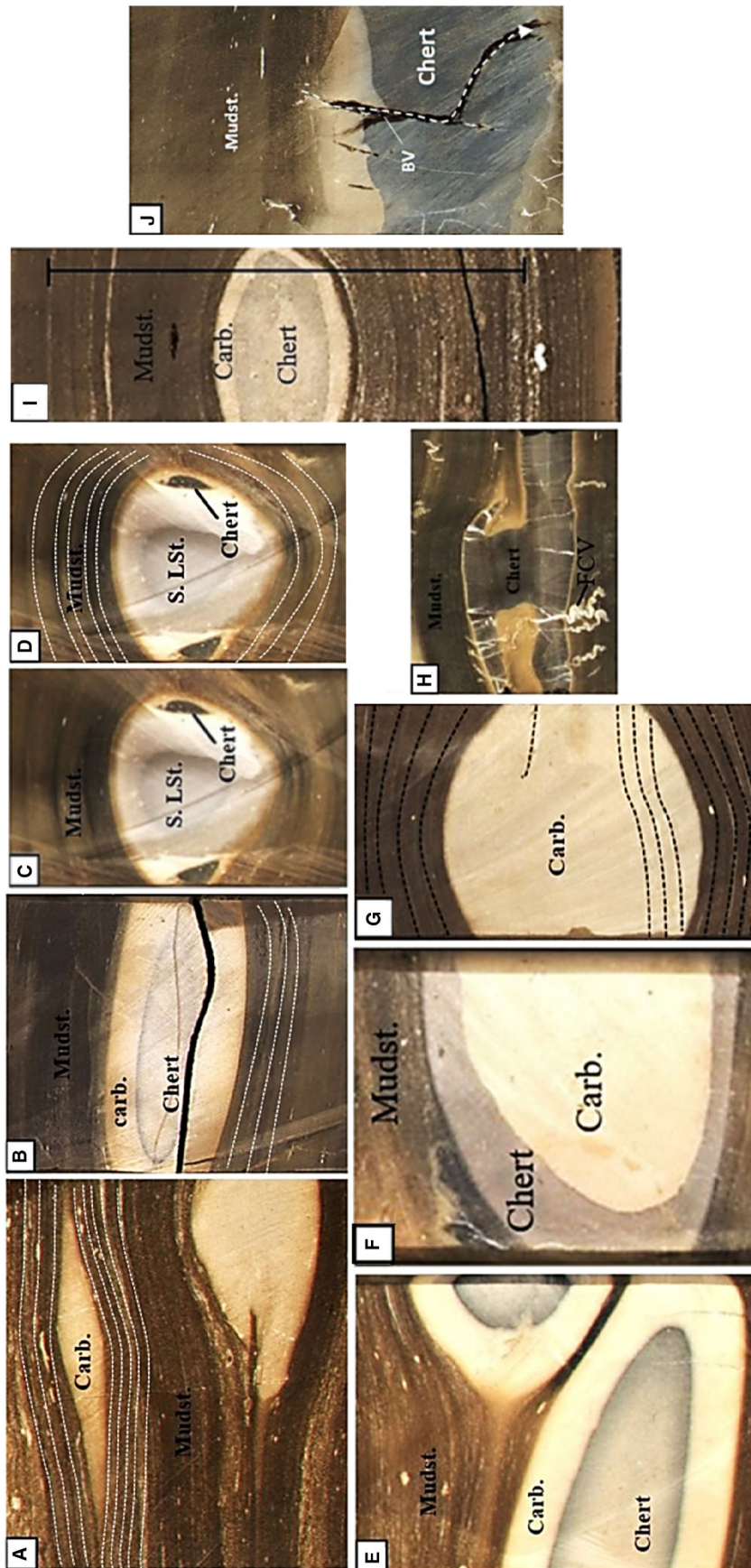
Fig. 2. Examples from the cores of the different types and shapes of carbonate and chert concretions and their relationships with fractures. BV, Bitumen veins; Carb, carbonate; FCV, folded calcite vein; PCV, planar calcite vein; S. LSt., silicified limestone. (A) Lensoidal carbonate concretion in mudstone. (B) Tabular composite chert–carbonate concretion. (C) Silicified limestone concretion with chert filling triangle areas at the edges. (D) Same as (C), with dashed lines showing laminae bending around the concretion. (E) Elliptical composite chert–carbonate concretion. (F) A composite carbonate–chert concretion hosted by mudstone. (G) Spherical carbonate concretion preserves the sedimentary laminae. (H) Irregular chert concretion cross-cut by folded calcite veins and hosted by mudstone. Note the bending of the laminae around concretions in (G). (I) A clear example of the laminae bending (strain field) around concretions. Black line (35 cm) represents the strain field. (J) Chert concretion is surrounded by a halo and associated with bitumen veins. Core width is 10 cm in all photographs.
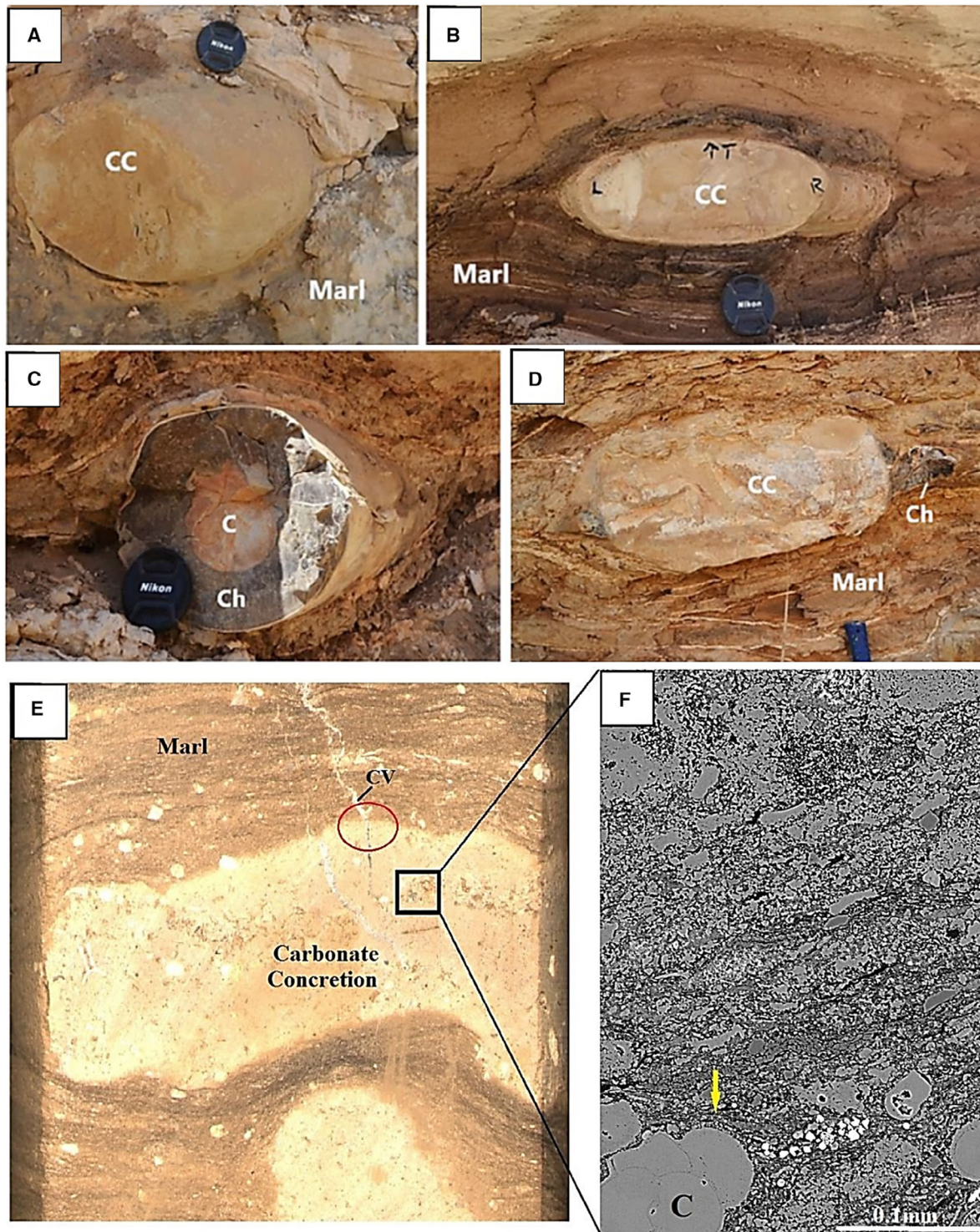
Fig. 3. (A) to (D) Field photographs showing examples of the different types of carbonate and chert concretions observed in the study outcrops. C, carbonate; CC, carbonate concretion; Ch, chert; Marl, phosphatic marl. (A) Spherical carbonate concretion in the Sultani Quarry (MCM). (B) Elliptical carbonate concretion in the Sultani Quarry (MCM). Lens cap is 5 cm. (C) Zoned carbonate-chert concretion in the Sultani Quarry (MCM). (D) Carbonate concretion with triangular shapes filled by chert at the edges in the Sultani Quarry (MCM). Hammer handle for scale (total hammer length 32 cm). (E) Core photograph of carbonate concretion in phosphatic marl interval from the Lower Unit (Al-Hisa Phosphorite Formation – AHP), Core C5. CV, Calcite Vein. Core width is 10 cm. Note the alignment of grains (laminae trace). (F) Backscattered electron (BSE) image of inset in (E) showing the bending of sediment around microfossils (yellow arrow).

morphology (Figs 2G and 3C). Lenticular carbonate concretions are rarely found in the study succession (Fig. 2A). 'Winged' carbonate concretions with chert filling triangular pinch points at the concretion margins (Figs 2C and 3D) are only found in lenticular forms. A few examples of carbonate concretions with irregular (asymmetrical) shapes were observed in the core.

Dimensions measured in the core are minimum estimates, given that most concretions were only partly intersected, but range from centimetres to decimetres. Outcrop examples allowed lateral examination of the different shapes of concretions, their dimensions and their relationship to the host rocks. Concretions observed at outcrop span a wide range of sizes, with diameters ranging from 15 cm to more than 3 m for carbonate concretions, and from 10 to 60 cm for chert concretions (Fig. S4). The horizontal concretion spacing in individual beds ranges from several centimetres to several metres (Fig. S4), with an average spacing of 2 m for carbonate concretions and 20 cm for chert concretions in all localities. Different concretion horizons exhibit a range in their horizontal spacing characteristics, due, for example, to possible differences in sites of nucleation, pore water composition, flux or dominant mode of solute transport (Chan *et al.*, 2007).

Relationships to host rock

The relationship between concretions and sedimentary structures (layering, lamination) in the host rocks is critical for establishing the mode of growth (Sellés-Martinez, 1996; Gaines & Vorhies, 2016). Sedimentary laminae can be traced from the host laterally into many of the observed carbonate concretions (Fig. 2G); suggesting a replace growth mode for these concretions (Raiswell, 1971; Gaines & Vorhies, 2016). In this type of concretion (Type I-carb; Fig. 4), the concretions usually show symmetrical (regular) morphologies with the laminae folding around concretions in relatively symmetrical patterns in the vertical plane. This symmetrical folding in the surrounding laminae is mainly observed where there are similar bed thicknesses in the stiffer layers directly above and below the concretion. The pattern of folding around these concretions is interpreted as evidence for differential compaction around the concretions, and is further taken to suggest early diagenetic growth of the concretions in relatively unconsolidated sediment (cf. Lash & Blood, 2004).

In Type II-carb concretions (present in the AHP Formation), the concretions exhibit irregular morphologies (Figs 2C and 5), laminae and sedimentary features are not generally observed in the concretionary body, although thin traces of original chert laminae may define distinct concretion increments (Fig. 5B and C). In these examples, the original chert bed can be seen to split into two or more displacive limestone concretion units (for example, DG1–4) in Fig. 5B.

Type I-chert concretions usually preserve original laminae and sedimentary structures and exhibit compactional deformation of host laminae, conforming to diagnostic indicators of replace growth (Raiswell, 1971; Sellés-Martinez, 1996; Lash & Blood, 2004; Gaines & Vorhies, 2016; Hooker *et al.*, 2017; Abu-Mahfouz, 2019).

Type II chert concretions are characterized by reaction rims around the periphery of concretions (Abu-Mahfouz *et al.*, 2020) and lack the compactional deformation of enclosing sedimentary laminae (Fig. 2J). These authors consider Type II-chert as forming at a later diagenetic stage.

Several remarkable examples of symmetrical (Type I-carb) and asymmetrical (Type II-carb) carbonate concretions are seen in the AHP outcrop in distinct concretion horizons (see Figs 4 and 5). In such examples, the bedding laminations can be easily traced through the concretion, but with an increased bed thickness compared to the adjacent bed. In these cases, the host bed deformation reflects the differential compaction around the concretions (Figs 3B and 4), where beds exhibit thinning and bending around the concretion. This geometry implies early replace concretion growth (Raiswell, 1971; Sellés-Martinez, 1996; Lash & Blood, 2004; Gaines & Vorhies, 2016). Irregular concretions (Type II-carb) appear to push the laminae apart in asymmetrical geometries, suggesting a displacive concretion growth (Sellés-Martinez, 1996). Such concretions have no sedimentary structures preserved inside the concretion body, and they usually show asymmetrical folding of the beds surrounding the concretion (Figs 5A, 8 and S5). However, where multiple displacive growth units have developed within individual chert beds, traces of original chert may be preserved (Fig. 5B).

Relationships to fracturing

Both carbonate and chert concretions are, in many cases, observed to be associated with natural fractures, particularly for those concretions
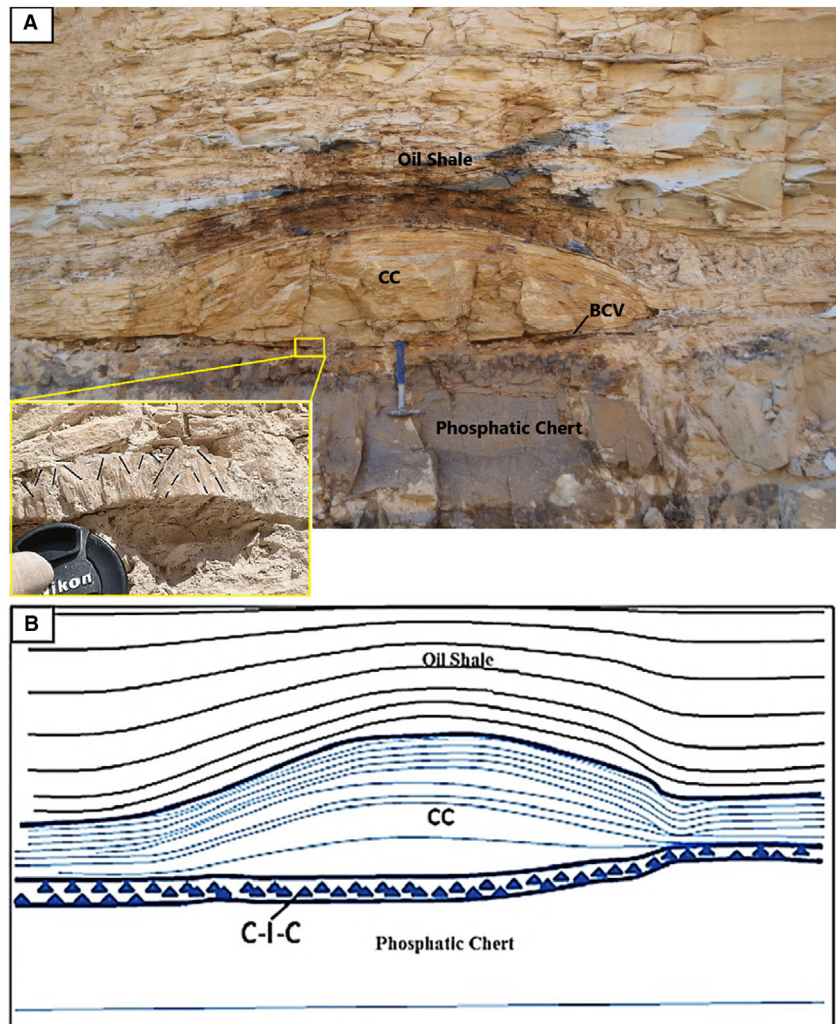
Fig. 4. (A) Carbonate concretion (Type I-carb) in the Qatrana Roadcut (Al-Hisa Phosphorite Formation – AHP) preserves the primary laminae entirely in the concretion body. The yellow rectangle is a close-up of the cone-in-cone structure in the bedding-parallel vein enveloping the concretion. (B) Drawing of (A). Hammer length 0.45 m, lens cap is 5 cm.

that exhibit irregular (asymmetrical) morphologies (Figs 2H, 2J, 5 and 8). Three main relationships between fractures and concretions were observed: (i) fractures confined to the concretion body; (ii) fractures that fan around the concretion with the folding of the overlying or underlying layers maintaining orthogonal relationships with those layers; and (iii) fractures that transect from the host the concretion body (Figs 2, 5A, 7, 8 and S5). In the latter, fractures generally terminate towards the concretion centre, with the highest fracture aperture at the concretion margin tapering towards a tip at the concretion centre (Fig. 2J). In such cases, fractures are always cemented.

Septarian fractures
Type II-carb concretions often exhibit a 'septarian' structure (Fig. 7A), with cemented fractures cutting across the concretion core. These

septarian fractures were observed in carbonate concretions restricted to specific concretion horizons in the lower interval of MCM. They are present as a single fracture or as a network of interconnected fractures, and usually tend to cluster at the concretion centre (Raiswell, 1971; Astin, 1986) and taper towards the concretion margins (Fig. 7A).

Folded calcite veins
Early undeformed, straight calcite veins were observed in cores to cross-cut Type I-ch concretions and continue with folded tips in the adjacent host beds (Fig. 2H). These externally folded calcite veins are interpreted to have formed at an early stage and folded by subsequent sediment compaction resulting from volume change caused by silica diagenesis (Abu-Mahfouz, 2019; Hooker et al., 2019). Their cross-cutting relationships with Type I-ch concretions indicate an
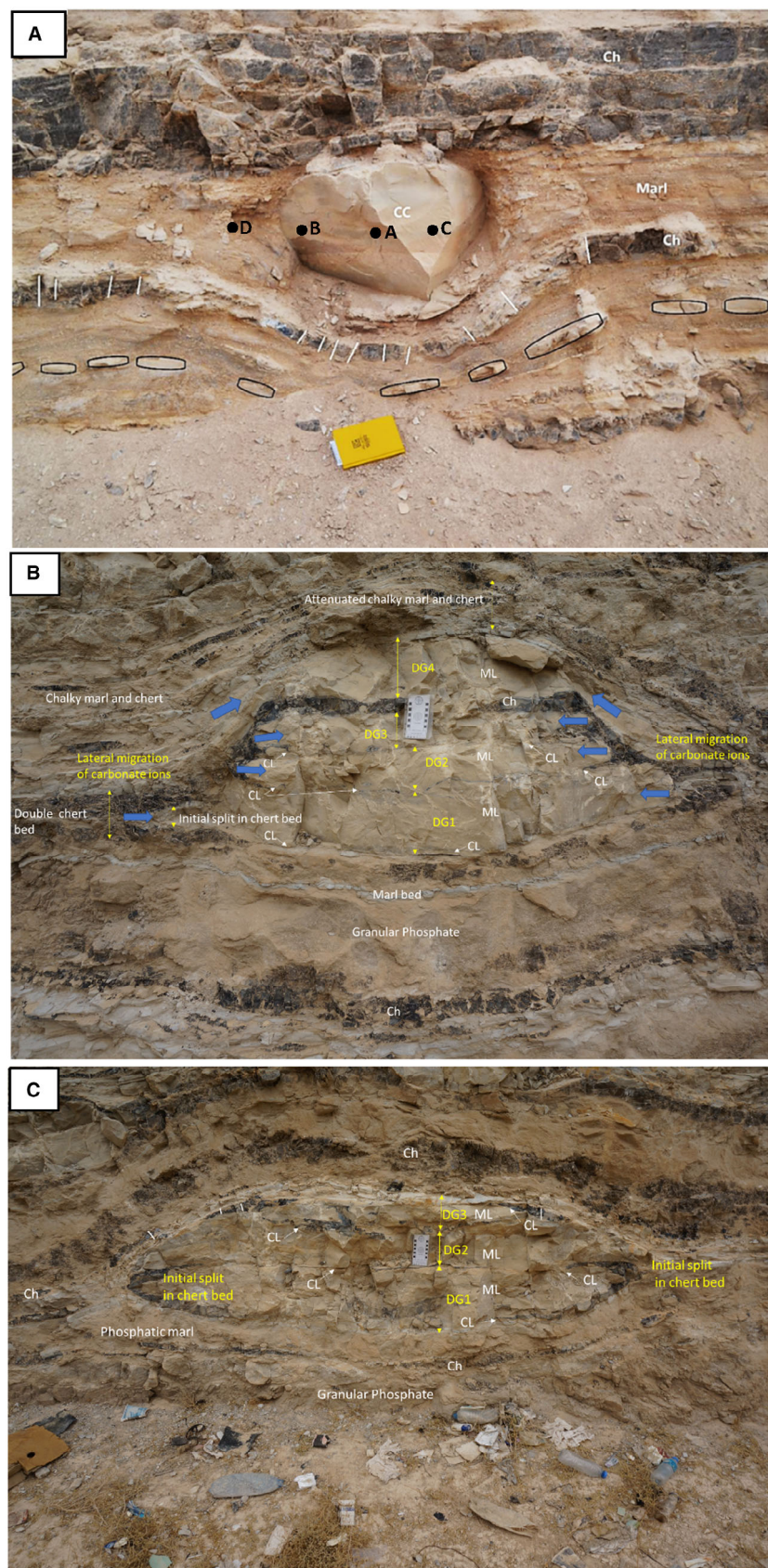
Fig. 5. Field photographs showing carbonate concretions displaying displacive growth in the Qatrana roadcut, Al-Hisa Phosphorite Formation. (A) Carbonate concretion (Type-II carb) with an asymmetrical bending of thin chert beds around the concretion body. Note the orientation of silica veins (white lines) in the chert beds and the bending of the small-concretion horizon (black elliptical shapes). ('A' to 'D') Sample points (see Fig. 10). Notebook for scale is 12 x 19 cm). (B) Asymmetrical Type-II carbonate limestone concretion showing displacive growth phases (DG1 to DG4). Note the relatively slightly disturbed underlying bed of granular phosphate and marl that acted as a constraining bed during concretion growth. Lateral migration of carbonate ions resulted in the splitting of the original double chert bed along marl partings into three displaced growth units (DG1 to DG3) comprising microcrystalline limestone (ML) and marked by thin chert lamina (CL). A higher growth unit (DG4) was, in turn, constrained by the top chert at the base and is overlain by thinned host rocks on the crest of the fold. Concretion growth thickness in units DG1 to DG3 is in the order of 4:1 compared to the original chert bed. Scale increments on the scale, 1 cm. (C) Near-symmetrical Type II – carbonate displacive limestone concretion showing three displacive growth units (DG1 to DG3) comprising microcrystalline limestone (ML). The underlying bed of granular phosphate/phosphatic marl acted as a constraining bed during concretion growth so that concretion is not exactly symmetrical. The split in the original chert bed is seen on both sides of the concretion; growth phases are delineated by thin chert tracer laminae (CL). White lines illustrate the orientation of early-formed silica veins. Concretion growth thickness in units DG1 to DG3 is in the order of 4:1 compared to the original chert bed. Ch, chert. Scale increments on the scale, 1 cm. CC, carbonate concretion; Ch, chert; CL, chert lamina; DG1-DG4, displacive growth stages; ML, marly limestone.
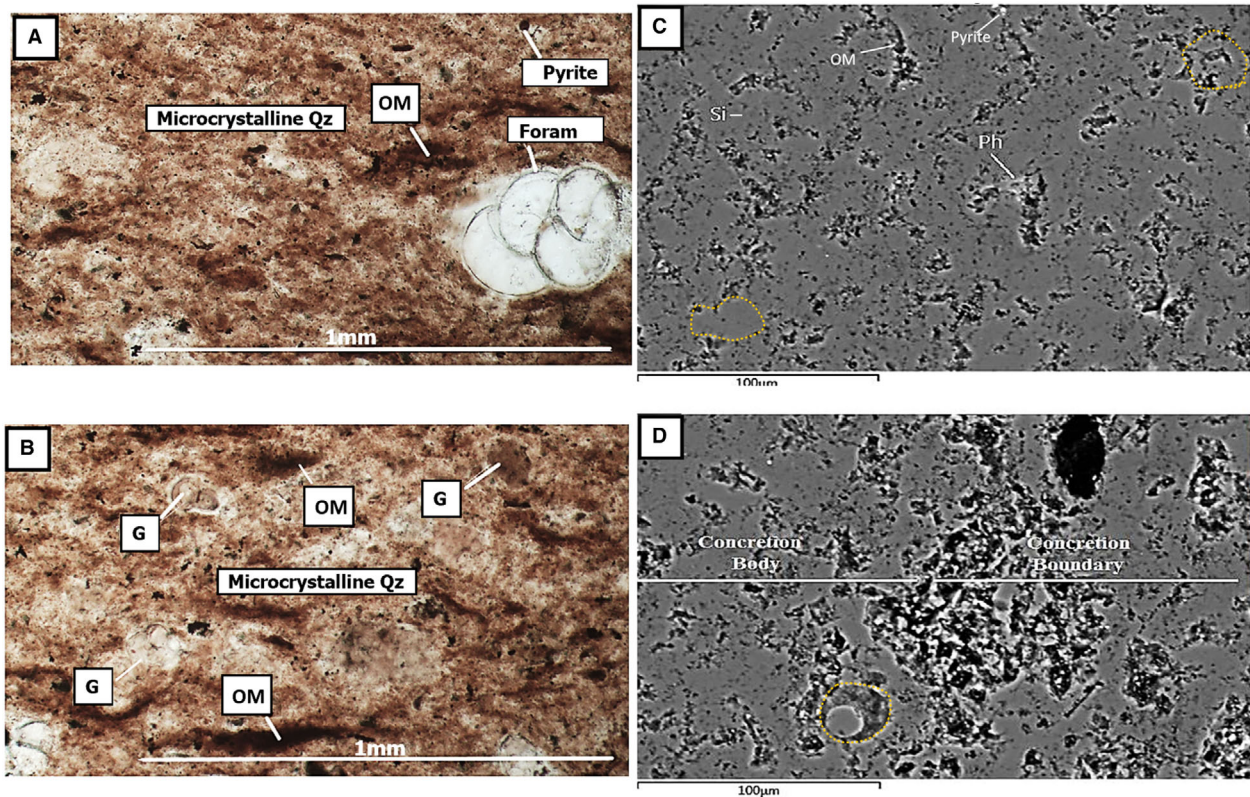
Fig. 6. (A) and (B) Photomicrographs showing a range of features observed inside the chert concretions, including well-preserved (un-compacted) foraminifera and fossil ghosts ('G'). (C) Backscattered electron (BSE) image of chert concretion from the Lower Unit, Core 13. Note that Silica represents >90%. Orange-dotted shapes show 'ghosts' of Radiolaria and foraminifera. OM, organic matter; Ph, phosphorite; Si, silica. (D) BSE image showing the gradational boundary of the chert concretion.

early formation of these concretions (Abu-Mahfouz *et al.*, 2020). Type II-ch concretions were observed to be cross-cut by, or associated with, bitumen veins (Fig. 2J).

Silica veins
Silica veins are confined to the chert beds in the AHP in the Qatrana outcrop where they are associated with Type II-carb concretions (Figs 5A and S5). These veins are consistently oriented orthogonal to the bed boundary, and they fan with the folding of the chert beds around concretions, displaying a 'radial' vein orientation (Figs 5A and S5B to D). Vein apertures are larger in the areas of greatest fold amplitude (average width 0.8 cm) around concretions, compared with the apertures of veins present in undeformed parts of the host rock layers (average aperture size of 2.9 cm; Fig. S5E and F).

Late calcite and gypsum veins
Calcite veins were also observed to be associated with carbonate concretions in the outcrops (Fig. S5C and D). These veins are planar with small apertures (average of 1.1 cm). They range from a few centimetres to a few metres in length and commonly cross-cut both Type I-carb and Type II-carb concretions and their respective host rocks, suggesting that these veins are late, and post-date the formation of both concretion types.

Fibrous, bedding-parallel calcite veins (in the Qatrana outcrop; AHP) and others filled by gypsum (in the Sultani quarry; MCM) were observed to curve around carbonate and chert concretions concordantly with the deformed bedding maintaining a consistent fibre direction (Figs 4 and 7B). Other examples show bedding-parallel gypsum veins cross-cutting carbonate concretions (Fig. S6), implying a late development
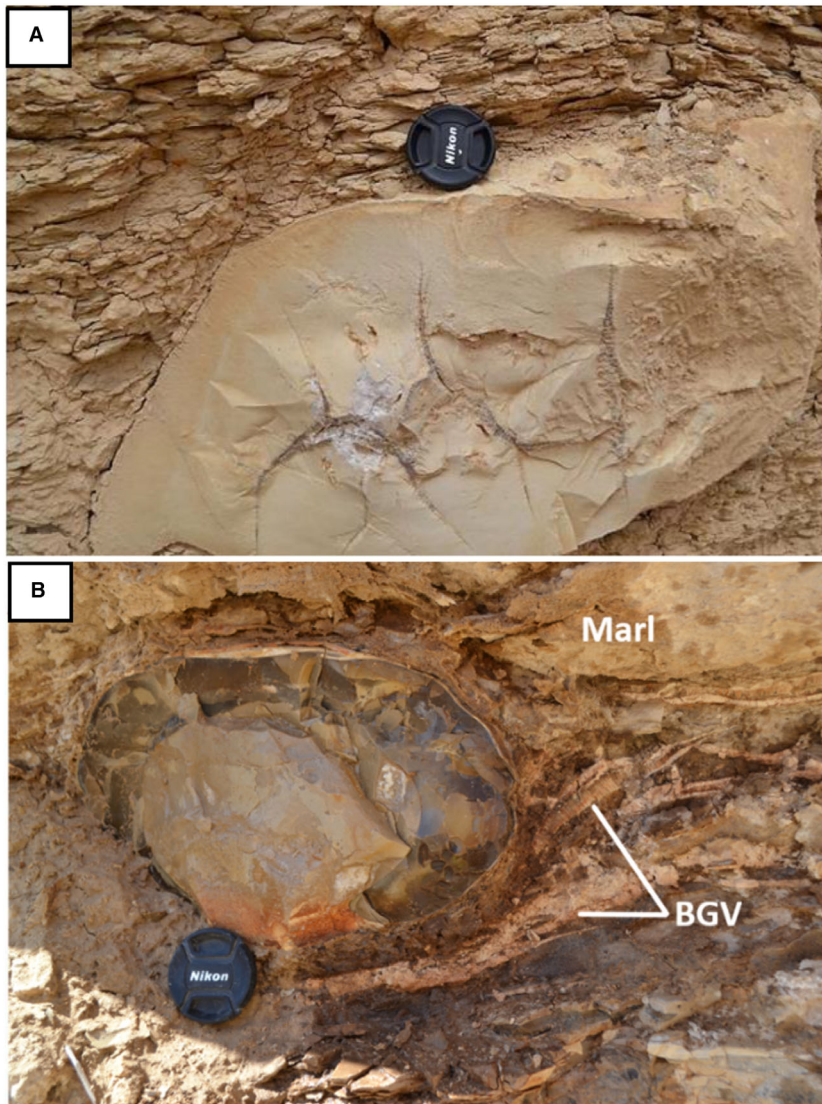
© 2023 The Authors. *Sedimentology* published by John Wiley & Sons Ltd on behalf of International Association of Sedimentologists., *Sedimentology*, **70**, 1521–1552

Fig. 7. (A) Septarian fractures in displacive carbonate concretion in the Sultani Quarry (MCM). (B) Bedding-parallel gypsum vein bending around a composite concretion composed of a concentric zonation of carbonate and silica. BGV, Bedding-parallel gypsum veins. Lens cap is 5 cm.

of these gypsum veins, post-dating the concretion formation.

Open fractures (barren or partially-cemented fractures) are also observed confined to the chert beds that are folded around Type II-carb concretions (Fig. 8) in a similar manner to silica-filled veins These open fractures occur in the highly deformed parts of beds, but with apertures exhibiting a narrow range of 0.8 to 1.0 cm.

Folding associated with concretions

Carbonate and chert concretions are generally associated with thinning (attenuation) and symmetrical folding of the overlying and underlying beds (Figs 3B, 4 and 5B), particularly around those concretions that exhibit symmetrical morphologies (Type I-carb, Type I-ch and Type II-ch). However, Type II-carb concretions in the AHP are usually associated with asymmetrical folding of the host beds/laminae such that fold amplitude is either greater or smaller in beds above relative to those below the concretion (Figs 5A to 5C, 8 and S5).

An important factor in the shape of the host rock folding associated with the concretions is the relative stiffness of the beds comprising the immediate host sediments. Host sediments of Type II-carb concretions, for example, are characterized by strong contrasts in the distribution of layer stiffness related to the presence and thickness of bedded cherts. Wherever chert beds exhibit different bed thicknesses around the Type II-carb concretion, the thinner chert and chalky marl beds exhibit larger fold amplitude than the thicker chert beds (Fig. 5A). This
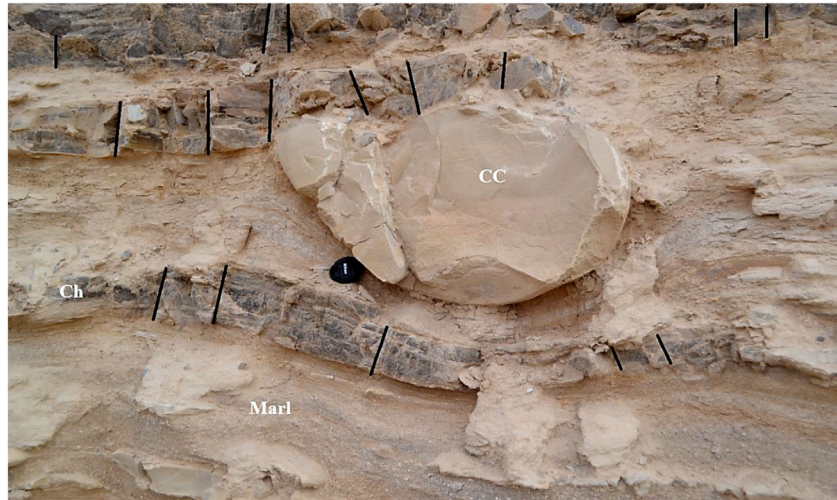
Fig. 8. Field photograph showing open fractures/joints (black lines) in chert beds bending around a displacive carbonate concretion in Al-Hisa Phosphorite Formation, Qatranah road cut. CC, Carbonate Concretion; Ch, Chert. Lens cap is 5 cm.

suggests that the gross fold geometry of the chert beds, around Type II-carb concretions, is dependent on the constraining effect of thicker (early lithified) chert beds that resulted in greater mechanical strength, thus impeding vertical deformation (either above or below).

MICROSCOPIC CHARACTERIZATION

Host rock

The studied interval consists of variable proportions of calcite, quartz, organic matter and apatite, with local amounts of chalcedony, dolomite, minor pyrite and sphalerite. Magnesium smectite is typically a minor component (<3%) that occurs in the marl intervals. Clay occurs in minor amounts (<5%). Minor Mg smectite is usually observed to be intergrown with calcite and micro quartz.

The organic particles show no visible structure and are typically sulphur rich. Bitumen-filled microfossils are abundant in the host rock in the MCM (Fig. S3).

Chert concretions

Chert concretions (Type I-ch and Type II-ch) sampled from the cores and outcrops are composed mainly (*ca* 95%) of microcrystalline quartz (Fig. 6 and Fig. S7). Small amounts (5%) of calcite, pyrite and fluorapatite are locally present (Fig. 6A to C). Traces of organic matter are also observed as an amorphous texture in thin sections. Silica-cemented radiolaria and foraminifera

tests are occasionally observed in Type I-ch concretions (Fig. S7). At the margin and outside these Type I-ch concretions, microfossils, including well-preserved foraminifera, are cemented by calcite (Fig. 6A and D). These concretions mainly show passive cementation of sediment, where cement normally occupies the pore space. These Type I-ch concretions also typically display gradational boundaries (Fig. 6D).

Most of the Type I-ch concretions examined in the study succession exhibit preserved traces of laminae, sedimentary structures and 'ghosts' of fossils (Fig. 6). These are diagnostic textural features that are generally taken to imply replacive alteration of the original carbonate grains by microcrystalline quartz (Maliva & Siever, 1988; Sellés-Martinez, 1996; De Craen *et al.*, 1998; Raiswell & Fisher, 2000).

Type II-ch concretions exhibit preserved laminae and sedimentary structures and have transitional boundaries with the host rock (Fig. 2J), which also conform to diagnostic criteria of replacive concretion growth (Sellés-Martinez, 1996). The overall texture in Type II-ch concretions suggests a progressive process of silicification that appears to have occurred during or after calcite cementation of microfossil tests (Abu-Mahfouz *et al.*, 2020).

Carbonate concretions

Carbonate concretions (Type I-carb and Type II-carb) are composed mainly (>90%) of calcite and show a microcrystalline texture (Figs 9 and S3). The calcite microcrystals are distributed in a very fine-grained matrix (Figs 9 and 10). The matrix
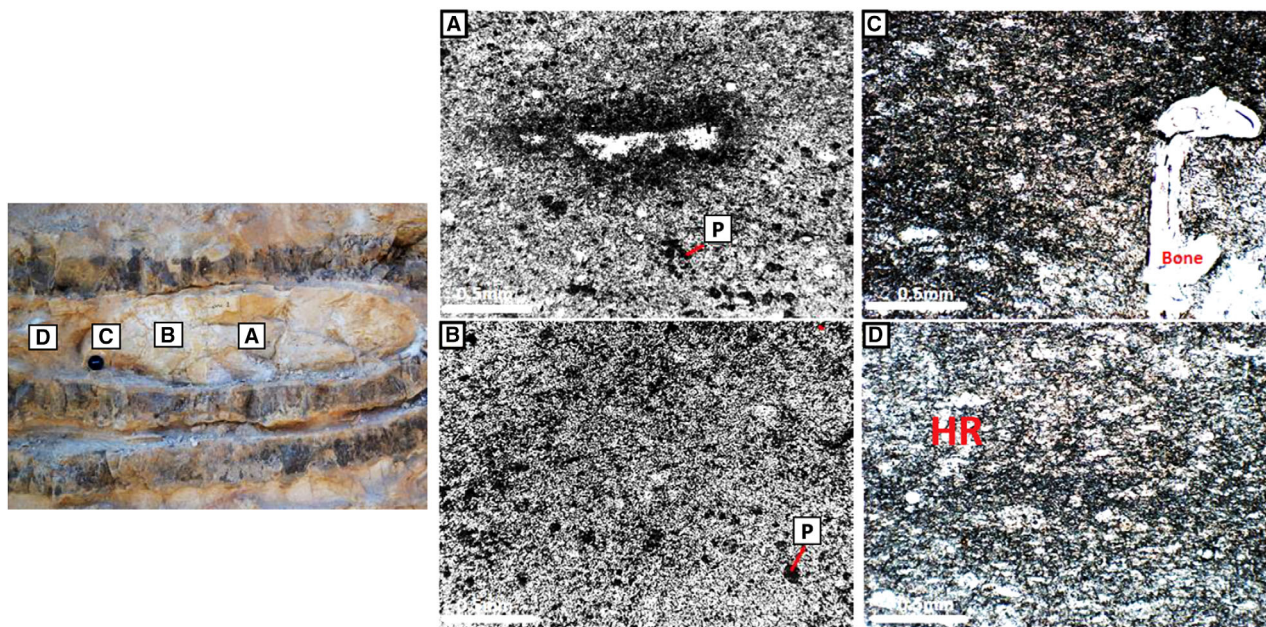
Fig. 9. Microphotographs of a systematically sampled (centre to edge) displacive carbonate concretion (Al-Hisa Phosphorite Formation, field photograph on left) showing the change in porosity, grain size and amount of cement from the centre (A) towards the margin of the concretion (C). HR, host rock; P, pore space. Note the decrease in the size of pore spaces from the centre towards the edge. Note the preserved bone fragment in (C) and the aligned grains in laminae in the host rock (D).
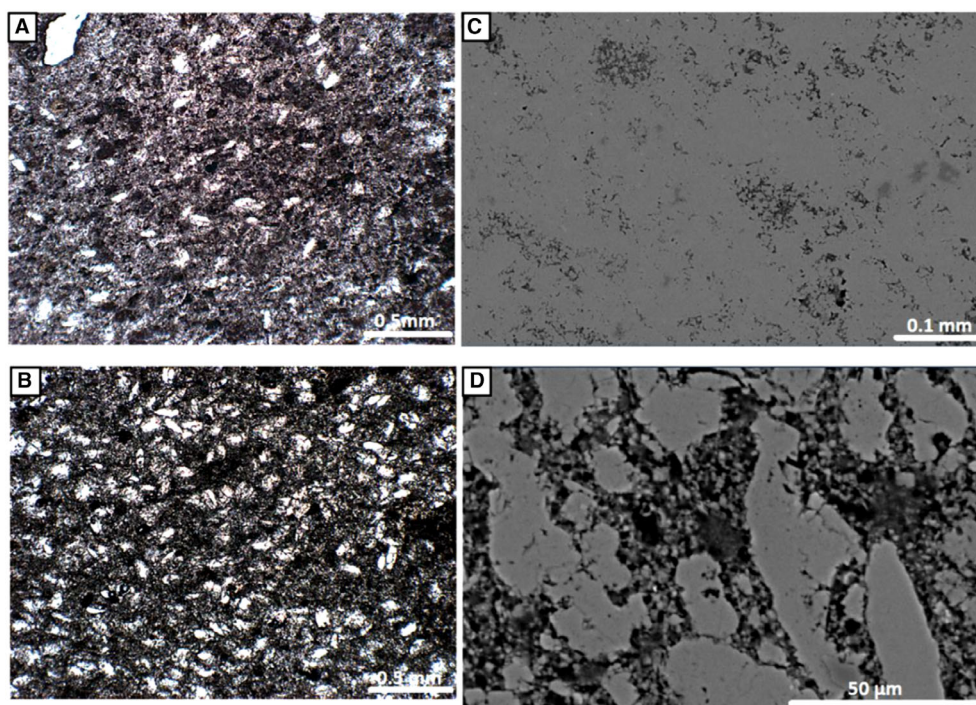
Fig. 10. (A) and (B) Microphotographs showing the composition of a systematically sampled, displacive carbonate concretion (Al-Hisa Phosphorite Formation). Note the multiple directions of the randomly aligned semi-fibrous calcite crystals. (C) Backscattered electron (BSE) image showing the texture of the concretion. (D) BSE image showing the texture of the host rock (chalky marl) that abuts the concretion. Locations of the samples (A) to (D) are shown in Fig. 5A.
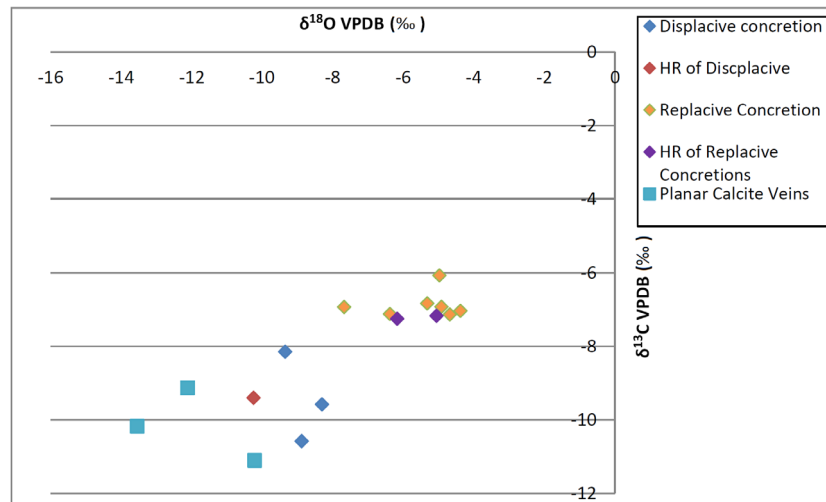
Fig. 11. Plot of stable isotope data of carbonate concretions and planar calcite veins transecting the concretions. VPDB = Vienna PeeDee Belemnite.

includes bioclasts, coccolith platelets, and microcrystalline low-Mg calcite cement and calcite crystals cementing fossil remains and foraminifera tests (Fig. 3E and F). The calcite is of both detrital and authigenic origin, although it is hard to infer the exact amount of the authigenic material due to the recrystallization of the matrix. Apatite occurs in cavities of fossil fragments (Fig. S3). Microfossils and fish/vertebrate bone remains are preserved as relatively undeformed bioclasts inside Type I-carb concretions (Fig. 9A and C).

In Type I-carb concretions, sedimentary laminae are traceable as aligned grains where the laminae can be traced as alternating dark and light bands (Figs 3F and 9). These concretions usually exhibit gradational boundaries. Planar calcite veins are observed to cross-cut these concretions, indicating that the concretion formation pre-dates the development of these veins.

In contrast, Type II-carb concretions are observed in thin sections to show no preserved sedimentary structure/lamination in the matrix calcite crystals in the form of micro-spar (at the microscopic sale) and show unaligned patterns (Fig. 10), suggesting a displacive mode of growth (Huggett, 1994; Liu *et al.*, 2019). This type of concretion usually exhibits a sharp boundary with the host sediments. However, where displacive growth has split an original chert bed along marl partings, thin laminae of the original chert can be traced through the displacive carbonate concretion thus partitioning growth units (Fig. 5B and C).

Systematic microscopic examination of carbonate concretions (Type I-carb and Type II-carb), from centre to edge, also shows that the calcite crystal size, porosity and percentage of cement change with distance from the centre. In general, the size of calcite crystals increases towards the concretion margins (Figs 9 and 10).

Point count-based microscopic investigation of both types of carbonate concretion shows that the percentage of cement fraction ranges between 70% and 80%, suggesting an early development of these concretions, which is consistent with previous diagenetic histories for the JOS (Powell & Moh'd, 2012; Huggett *et al.*, 2017).

STABLE ISOTOPE ANALYSIS

The stable isotope data of both the Type I-carb and Type II-carb concretions and their associated calcite veins are shown in Table 2. The carbon isotopic ratios of both concretion types exhibit a relatively narrow range of samples analysed from the centre to the edge of each type of concretion ($\delta^{13}C$ values range from −7.13 to −6.07‰ for Type I-carb and from −10.58 to −8.15‰ for Type II-carb; Table 2; Fig. 11). However, the results show that the edges are more depleted in carbon $\delta^{13}C$ than the centres. In general, the $\delta^{13}C$ isotopic signatures of the centres (−8.15 to −6.83‰) of the concretions analysed are closer to those of the host rock samples (−9.40 to −7.17‰), implying an organic origin
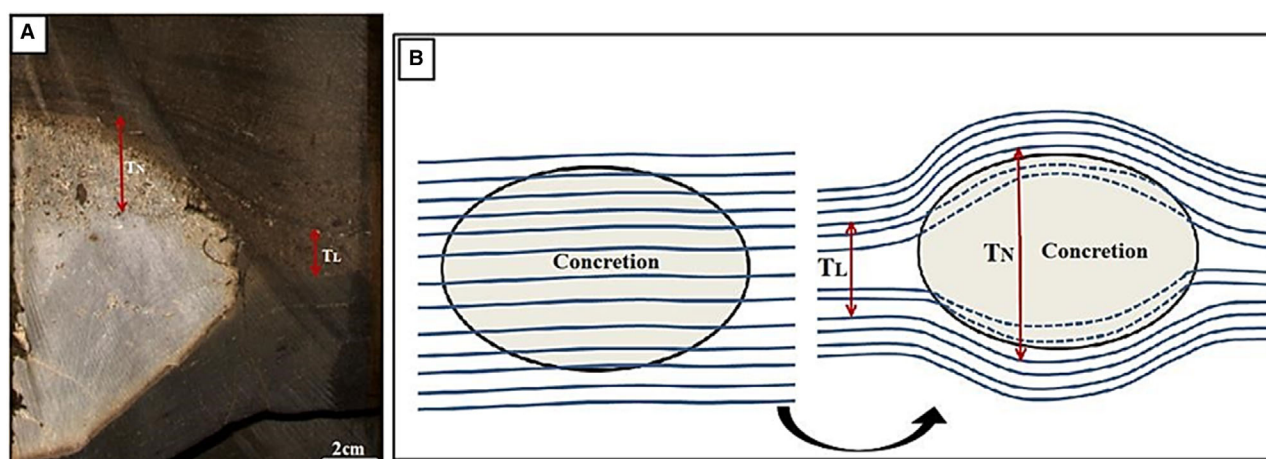
Fig. 12. Quantification of compaction around replacive concretions. TN, un-compacted bedding thickness (thickness between the beds immediately above and below concretions); TL, compacted bedding thickness (thickness between same horizons, lateral to the concretion). (A) Core photograph of carbonate concretion showing differential compaction around a replacive concretion. (B) Illustration of laminae before and after compaction. Compaction ratio is (TN/TL).

of the carbon (Hesslebo & Palmer, 1992; Yoshida et al., 2018). This suggests that the source of the isotopically light carbon was likely either directly from the decomposition of organic matter (for example, within the zone of sulphate reduction) or biogenic methane (Irwin et al., 1977), which could be derived locally or possibly from underlying strata (for example, phosphate or organic phytoplankton-rich marl).

The oxygen ($\delta^{18}O$) isotopic values range from −9.35 to −4.38‰ of all the analysed Type I-carb and Type II-carb concretions. These $\delta^{18}O$ isotopic compositions suggest that the concretion formation commenced at shallow burial depth (low temperature of precipitation), but continued during progressive burial (Raiswell, 1971; De Craen et al., 1998; Raiswell & Fisher, 2000; Woo & Khim, 2006; Marshall & Pirrie, 2013; Gaines & Vorhies, 2016). The $\delta^{18}O$ ratios also suggest that the precipitation occurred not far under the sediment–water interface mainly from CO_2 produced by sulphate-reducing bacteria (Irwin et al., 1977).

The carbon isotopic values of planar calcite veins transecting Type I-carb and Type II-carb concretions range from −11.1 to −9.13‰, indicating that the veins are more depleted in carbon than the concretions and the host rocks (Fig. 11). Taken together with their cross-cutting relationship these results indicate that the planar calcite veins formed at a late stage, probably during tectonic uplift.

STRAIN ANALYSIS AROUND CONCRETIONS

Strain analysis offers an opportunity to examine the amount of deformation that rock units have undergone during burial and uplift (Fossen, 2016). It also provides significant information about the mechanisms of deformation. Primary, unconsolidated sediments compact through progressive burial and associated dewatering (Garrison, 1981), or when undergoing diagenesis and lithification in different degrees. Many deformational features such as layer thinning and bending around concretions, stylolite formation or deformation of pre-existing structures can be attributed to compaction.

Strain was measured in the present study around the different types of concretions. The distinctive appearance of lamina boundaries in the beds that host concretions provides good visual markers for original depositional relationships (Fig. 12A and B) and thus allows a unique opportunity to calculate the degree of compactional strain around a given concretion (Hooker et al., 2017). Exposures in quarries and roadcuts allowed the patterns and extent of the folding associated with concretions to be assessed in detail, allowing analysis of the relative timing of growth, and differentiation of different growth modes.

Two types of strain fields were observed in both the core and outcrop: (i) a symmetrical

strain field, where beds are deformed in a vertically symmetrical manner around concretions (Figs 2A, 2I, 3B and 12); and (ii) a vertically asymmetrical strain field (Type II-carb), where concretions show vertically asymmetrical degrees of localized folding, and deformed beds show higher curvatures and amplitudes around concretions (Figs 5, 8 and S5). In the latter, the beds appear to have been folded due to a forced folding process with space in the host rocks lost to make way for the concretions as distinguished from differential compaction. More competent, mechanically isotropic beds such as thick chert or granular phosphate are seen to constrain the asymmetry of many of the Type II-carb concretions in the heterolithic AHP (Fig. 5).

Compaction strain analysis, which is related to the symmetrical strain field, was performed around Type I-ch, Type II-ch and Type I-carb concretions. The compaction, in this case, is represented by the deformation occurring in the lamina thinning around concretions due to differential compaction processes governed by gravity (Fig. 12A and B). The compaction ratio of the thicknesses of the deformed beds in the strain field was measured, both within and around concretions and in the undeformed part of the same beds. The strain shadow, the deformation zone around the concretion (Lash & Blood, 2004, 2007), disappears within a distance up to 2 m above and below the concretion.

According to Hooker *et al.* (2017), the concretion compaction ratio (CN) for replacive concretion can be calculated as follows:

$$C_N = T_N / T_L$$

where:

T_N: is the original thickness of a stratigraphic package across the concretion vertically.

T_L: is the compacted thickness of the same package lateral to the concretion.

The results of the compaction strain analysis are displayed in Tables 3 and 4. Compaction ratios quantified, from the core, for the Type I-ch and Type II-ch concretions display an average of 2.18, whereas the average compaction ratio for the Type I-carb concretions is 3.33.

The compaction ratios, in the outcrops, of the Type I-ch and Type II-ch concretions, are lower (average of 2.5) than those for the Type I-carb concretions (average value of 3).

In the case of displacive concretions (i.e. Type II-carb), where the strain field is considered asymmetrical, the strain is described as the deformation of the forcibly folded beds around concretions. However, compaction strain analysis was not applicable around these Type II-carb concretions because this method only applies to differential compaction, for replacive concretions.

CONCRETION CLASSIFICATION BASED ON THE MODE OF FORMATION

Based on the above-described macroscopic and microscopic textural characteristics of the four different concretion types observed in the study interval and their influence on host rock laminae, two main types of concretions were identified based on their growth mode (i.e. formation mechanism): replacive concretions and displacive concretions (Table 1). Replacive concretions are those that display regular morphologies, ghosts of microfossils and infilled porosity, and well-preserved primary sedimentary structures and laminae within the concretion body, indicating a replacive growth mechanism (Maliva & Siever, 1988; Sellés-Martinez, 1996; De Craen *et al.*, 1998; Raiswell & Fisher, 2000; Gaines & Vorhies, 2016). In this type of concretion growth, the strain field around the concretion body is symmetrical. Based on the above, replacive growth is observed in Type I-chert, Type II-chert and Type I-carb concretions.

In contrast, displacive concretions are usually observed as irregular shapes and show sharp contact with the host rock, random crystal arrangements and no internal sedimentary structures (Huggett, 1994; Liu *et al.*, 2019), although they may preserve traces of primary chert laminae. The strain field around the concretion body in this type of concretion growth is asymmetrical. This mode of growth is mainly observed in Type II-carb concretions.

DISCUSSION

Concretion diagenesis and chemical conditions for concretion formation

The formation of both the silica and carbonate cement in the JOS is attributed to the effects of their dissolution/precipitation and pore fluid chemistry. Chert in the Upper Cretaceous–Eocene study interval has a biogenic silica origin, and it is thought to have formed by the replacement of diatoms, radiolaria and silicoflagellates by opal-CT, and then by quartz

Table 1. Major diagnostic indicators of replacive and displacive growth of concretions.

Concretion growth mode	Diagnostic indicators	
	Macroscopic evidence	Microscopic evidence
Replacive growth	Laminae and sedimentological features can be traced in the concretion body	Concretions usually exhibit microcrystalline internal structure
	Concretions have regular (uniform) shapes: mainly spherical and elliptical	Crystals are arranged in aligned patterns
	Concretion-associated fractures are rare	Preserved internal sedimentary structures and laminae
	Laminae deformed/thinned in a symmetrical vertical plane resulting in a symmetrical strain field due to differential compaction	Concretions exhibit transitional boundaries
Displacive growth	No traces of laminae and sedimentological features in the concretion body, but individual displacive units may be delineated by thin chert tracer beds	Concretions exhibit fibrous internal crystalline structure
	Concretions have irregular (non-uniform) shapes	Crystals are arranged in a random (un-aligned) pattern
	Concretions are associated with fracturing	Sedimentary structures and laminae are not preserved
	Laminae deformation is reflected by an asymmetrical vertical plane resulting in an asymmetrical strain field due to force folding	Concretions have sharp contact with host rocks
	Some concretions display triangular spaces filled by chert at their edges	Concretions have sharp boundaries

Table 2. Isotope data of carbonate concretions (including symmetrical and asymmetrical types), their host rocks and planar calcite veins transecting the concretions in the Qatrana roadcut. '1' to '4': centre to edge of the concretion through the host rock. VPDB = Vienna PeeDee Belemnite.

Sample	$\delta^{13}C$ VPDB ‰	$\delta^{18}O$ VPDB ‰	Growth
1	−8.145	−9.348	Displacive?
2	−9.577	−8.299	
3	−10.582	−8.881	
Host rock	−9.402	−10.239	
1	−6.923	−4.920	Replacive?
2	−7.032	−4.379	
3	−7.133	−4.678	
4	−6.072	−4.972	
Host rock	−7.171	−5.057	
1	−6.831	−5.320	Replacive?
2	−7.122	−6.379	
3	−6.931	−7.678	
Host rock	−7.250	−6.170	
Planar calcite vein	−10.180	−13.550	
Planar calcite vein	−9.131	12.120	
Planar calcite vein	−11.102	−10.210	

(Kolodny, 1969; Kolodny *et al.*, 1980; Moshkovitz *et al.*, 1983). This is supported by the presence of sphalerite as a pre-dominant early diagenetic sulphide mineral in the same interval as reported by Huggett *et al.* (2017). Zinc is necessary for the growth of diatoms (Varela *et al.*, 2011) and is released into the pore water when these organisms die and decay. This strongly supports the biogenic origin of the silica. The transition of biogenic silica from opal-A to opal-CT and subsequently to cryptocrystalline quartz is known to produce volumetric changes in semi-lithified silica-carbonate sediments (Kastner *et al.*, 1977; Isaacs, 1982; Murray *et al.*, 1992; Behl & Garrison, 1994) including deformation structures (Eichhubl & Behl, 1998; Davies *et al.*, 1999; Davies, 2005). This is considered to be the driving mechanism for brecciated fabrics in individual laminated chert beds and disharmonic folds in underlying chert-rich sequences (Powell & Moh'd, 2011: figs 19 and 20). Faster rates of opal-A to opal-CT transition have been observed in pure silica ooze layers as compared to those with a higher proportion of clay, and other detrital minerals (Bohrmann *et al.*, 1994) in Miocene sediments. Fracturing of chert sols and the development of gentle folding of the semi-lithified chert beds are interpreted as the result of volume changes associated with the expulsion of pore water during early diagenesis.

Table 3. Compaction measurements around replacive chert and carbonate concretions in the cores.

Chert concretion				Carbonate concretion			
Sample number	TN	TL	Compaction ratio (CN)	Sample number	TN	TL	Compaction ratio (CN)
1	5.0	3.0	1.67	1	20.0	5.5	3.64
2	3.0	2.	1.50	2	12.0	7.0	1.71
3	3.5	2.5	1.40	3	20.0	3.2	6.25
4	2.0	1.5	1.33	4	15.0	4.0	3.75
5	5.5	2.0	2.75	5	25.0	3.8	6.58
6	6.0	3.5	1.71	6	14.0	2.5	5.60
7	1.8	1.0	1.80	7	15.5	5.0	3.10
8	4.0	2.5	1.60	8	14.0	4.5	3.11
9	4.0	1.5	2.67	9	20.0	7.0	2.86
10	15.5	5.0	3.10	10	19.0	5.0	3.80
11	11.0	3.0	3.67	11	22.0	7.5	2.93
12	14.0	6.0	2.33	12	20.0	6.0	3.33
13	5.5	2.0	2.75	13	13.0	5.0	2.60
14	4.0	2.0	2.00	14	12.0	3.0	2.67
15	12.0	5.0	2.40	15	5.0	1.5	3.33
				16	5.0	2.0	2.50
				17	4.5	2.5	1.80
				18	4.0	2.0	2.00
				19	2.5	1.0	1.74
Average	6.45	2.83	2.18		13.82	4.11	3.33

Table 4. Compaction ratios measured around replacive chert and carbonate concretions from the outcrops.

Chert concretion				Carbonate concretion			
Sample number	TN	TL	Compaction ratio (CN)	Sample number	TN	TL	Compaction ratio (CN)
1	14.0	5.0	2.80	1	45.0	15.0	3.00
2	17.0	6.0	2.83	2	48.0	17.0	2.82
3	3.75	2.5	1.50	3	50.0	14.0	3.57
4	15.0	6.0	2.50	4	55.0	18.0	3.06
5	14.0	5.0	2.80	5	58.0	20.5	2.83
6	18.0	7.0	2.57	6	46.0	15.0	3.07
7	14.0	5.0	2.80	7	48.0	13.0	3.69
8	10.0	3.5	2.86	8	45.0	13.5	3.33
9	3.0	2.5	2.40	9	55.0	19.0	2.89
10	5.0	2.0	2.50	10	58.0	19.0	3.05
11	5.0	2.5	2.00	11	46.0	16.0	2.88
				12	50.0	14.0	3.57
				13	74.0	25.0	2.96
				14	210.0	60.0	3.50
				15	71.0	24.0	3.96
				16	80.0	25.0	3.20
				17	75.05	24.0	3.15
				18	60.5	14.0	4.32
				19	40.0	13.0	3.08
				20	39.0	15.0	2.60

Carbonate in the calcite cement in the study interval is interpreted to be derived from microbial diagenesis (decomposition) of organic matter, calcareous microfossils (for example, coccoliths) and phosphomicritization of shelly material (Soudry & Champetier, 1983; Powell & Moh'd, 2012). Calcium was derived from seawater (Hooker *et al.*, 2017; Huggett *et al.*, 2017). Dissolution of the host sediment may also have contributed significantly to the carbonate cement fraction in all types of concretions. This is evident by the narrow ranges of the stable isotopic values of the systematically analysed carbonate concretions and their host rocks (Fig. 11).

In the study succession, both silica and carbonate diagenetic processes are related to microbial diagenesis of organic matter and are closely linked in both time and space, with pH, presumably influencing whether silica or carbonate precipitates (Huggett *et al.*, 2017). According to these authors, most of the early diagenetic processes in the study succession are believed to have occurred within the first 10 m of burial. Early diagenesis of chert is also supported by penecontemporaneous brecciation fabrics in chert laminae in the lower part of the succession (Powell & Moh'd, 2011).

Silica and carbonate diageneses are usually inextricably linked (e.g. Kastner *et al.*, 1977; Torres *et al.*, 2020). It is argued that carbonate and silica ions were: (i) exceptionally mobile; and (ii) highly sensitive to one or more tipping points, favouring a switch from carbonate to silica precipitation (or vice versa), during diagenesis of the JOS. Kastner *et al.* (1977), among others, showed that silica solubility is strongly coupled to alkalinity and the availability of key cations such as Mg^{2+}.

It is well-recognized that the occurrence of certain ions in solution at neutral pH values enhances silica polymerization (e.g. Bisque, 1962; Sheikholeslami *et al.*, 2002). The rate of transformation of opal-A to opal-CT is found to be much higher in carbonate (for example, AHP) than in clay-rich (for example, MCM) sediments according to Kastner *et al.* (1977). Those authors also found that magnesium hydroxide is important for opal-CT formation. The carbonate dissolution plays a key role since it provides the necessary alkalinity and a proportion of the Mg^{2+}. Seawater, or dissolution of high-Mg bioclasts, provides extra magnesium for the magnesium hydroxide required for opal-CT polymerization (Kastner *et al.*, 1977; Huggett *et al.*, 2017). Mg^{2+} ions in pore waters may have

acted as a catalyst for quartz precipitation, contributing to the formation of chert concretions.

The following processes are proposed here to have operated during early diagenesis. (i) Carbonate concretions precipitated under closed-system conditions, where porewaters were rich in dissolved inorganic carbon (DIC), the latter derived from the dissolution of primary carbonate and degradation of organic matter (or oxidized methane from adjacent organic-rich sediments), and where the rate of DIC diffusion out of the system was sluggish, possibly confined by early lithified chert/phosphate beds, resulting in the preservation of primary carbonate and precipitation of carbonate concretions. (ii) Quartz concretions precipitated in a low-DIC system (potentially, but not necessarily, open) meaning that any primary carbonate was likely soluble and, therefore, catalysts for quartz precipitation were available (for example, Mg ions). Thus, the control on quartz versus carbonate precipitation was potentially simply related to the fluid flow conditions and DIC. Critically, closed system precipitation and/or preservation of primary carbonate implies concurrent retardation of transformation from opal-A to opal-CT (see Kastner *et al.*, 1977).

Thus, a process-oriented model could explain the development of the large asymmetrical and symmetrical Type II carbonate concretions (in the heterolithic AHP), which deform underlying and overlying chert/marl beds often asymmetrically, depending on the constraining mechanical strength of the surrounding beds. In Fig. 5A, the thick chert bed overlying the concretion is interpreted to have lithified first (by reaction of moderate to high alkalinity and catalysts derived from carbonate dissolution or from the overlying seawater). It is proposed here that the overlying early-lithified chert bed promoted closed system conditions in the underlying strata. The DIC accumulated in the underlying porous chalky marl beds, leading to migration of DIC ions to nucleation centres and precipitation of microcrystalline cement resulting in displacive carbonate concretion growth and, concomitantly, retardation of lithification of the underlying chert/marls beds. This resulted in a greater degree of (downward) deformation in the underlying beds.

Additional examples are shown in Fig. 5B and C. In Fig. 5B, the constraining bed is a thick bedded granular phosphate (with thin marl). The initial early lithified chert bed bifurcates (splits) along three thin marl partings allowing displacive carbonate ions to migrate from

adjacent carbonate-rich beds; three tabular-shaped units of microcrystalline limestone showing displacive growth (DG1 to DG3) are separated by traces of original thin chert laminae. Thin marl laminae within the chert beds appear to have been the loci for the lateral migration of carbonate ions in alkaline pore waters derived from the chalky marl interbeds resulting in vertical displacive growth (Fig. 5B and C). A higher displacive concretionary unit (DG4) was in turn constrained, below, by the thinned topmost chert bed resulting in upward asymmetrical growth during the migration of carbonate ions. Compactional thinning of the thin beds of chalky marl and chert above the composite concretion indicates that the latter formed relatively early during burial diagenesis.

Following on from this hypothesis, the concentric Type I-carb concretions may thus indicate transitions from high DIC (likely closed system) to low DIC (possibly open system) conditions or vice versa. The chemistry of the system was likely driven by high and unsteady rates of input of labile organic matter, biogenic silica and carbonate derived from the host sediments.

In carbonate concretions, especially Type II-carb concretions, the concretion growth is thought to have taken place about 5 to 10 m below the sediment–water interface in semi-lithified sediment (cf. Huggett *et al.*, 2017). This is demonstrated by the absence of hard ground or erosional surfaces on the crests of concretions indicating that these concretions were not exposed on the seafloor.

Early lithification of chert sols and the development of vertical fractures, some infilled by silica also demonstrate partial lithification sufficient to allow shrinkage fractures to develop at the sediment–water interface or at shallow burial depths. Fractures may have originated as syneresis cracks.

The origin of the microcrystalline carbonate cement in Type II-carb is enigmatic. The association of chalky marl and porcellanite beds interbedded with the chert and phosphate (Fig. 5B and C) indicates that carbonate ions were available during early diagenesis. Part of the bicarbonate required for concretion development may have been derived from the decomposition of microbial organic matter in these sediments, sourced either from organic phytoplankton in the marls or fish/vertebrate fragments in the phosphate-rich beds. Microbial activity is commonly seen in the granular phosphate beds associated with this lithofacies (Powell &

Moh'd, 2012; Gaines & Vorhies, 2016). The carbonate cement may also have been sourced from the dissolution of the host sediment (marine carbonate shells) at shallow burial depths.

Replacive versus displacive growth modes: diagnostic indicators

Previous studies of concretion growth have drawn attention to the two contrasting modes of concretion growth; namely replacive versus displacive. Sellés-Martinez (1996) and Gaines & Vorhies (2016) in particular, have reviewed diagnostic indicators for these two end members.

Sellés-Martinez (1996) stated that, in replacive growth, the concretion occupies the place of pre-existing material while growing. In such a growth mode, the cement is thought to replace the host material or passively fill the pore space (Sellés-Martinez, 1996; Marshall & Pirrie, 2013). The growth of concretions, in this case, results from super-saturation of DIC in porewaters, which in mudrocks, usually results from alkalinity created by microbial respiration of organic matter in the primary sediment (e.g. Sellés-Martinez, 1996). Gaines & Vorhies (2016) also showed, at the microscale, that in this mode of growth the carbonate ions integrate into a concretionary body by extensive cementation of pore spaces, reflecting a pore-filling mechanism (Raiswell, 1971). This leads to changes in the porosity of the sediment during the growth of concretions (Raiswell, 1971).

In replacive concretions, sedimentary laminae and structures can be clearly traced through the concretion body (Raiswell, 1971; Sellés-Martinez, 1996). Examples are clearly seen in the JOS Type I-ch, Type II-ch and Type I-carb concretions. Replacive concretions are seen at specific horizons in the outcrops (Fig. 4), core samples and relevant borehole images (Fig. 12A). The growth of replacive concretions is believed, here, to be strongly linked to symmetrical folding patterns (Fig. 3B and Fig. S8), particularly where there is little or no contrast in the host lithologies, for example homogeneous marl in the MCM. This is revealed by the deformation occurring in the lamina thinning around concretions due to differential compaction processes governed by gravity (i.e. symmetrical strain field).

Displacive concretions, in contrast, can be recognized by their massive nature with little or no preserved internal sedimentological features or laminae (Sellés-Martinez, 1996). However,

very thin chert tracer laminae may be preserved between separate displacive units in compound concretions (for example, Fig. 5B). This general diagnostic feature was observed (macroscopically and microscopically) in most of the JOS displacive concretions, in specific horizons within the heterolithic AHP. Displacive concretion growth was first recognized by Richardson (1921), who reported experimental deformation of bedding around concretions due to displacive growth. Saigal & Walton (1988) and Sellés-Martinez (1996) have also argued that fracturing of the host rocks around concretions is a major indicator of the displacive growth of concretions. This type of concretion is believed to form under shallow burial conditions (the first few metres of burial) and against the overburden load; displacive growth develops by force of micro-spar crystallization (Dewers & Ortoleva, 1990; Sellés-Martinez, 1996). The concretion starts to grow when oversaturation of parent brines is associated with un-cemented, highly porous hosts, which is only possible under shallow burial conditions or by early overpressuring of sealed beds (Sellés-Martinez, 1996) as in the case of thick constraining beds of phosphate or chert. Displacive growth requires the shear strength of the host to be very low (Sellés-Martinez, 1996). This growth mode may also occur during early burial diagenesis, which would only be possible if the host beds have enough plasticity (high fluid content) to allow deformation by the concretion growth (Sellés-Martinez, 1996).

Displacement occurs when beds are forced apart by the growth of minerals (Astin & Scotchman, 1988; Sellés-Martinez, 1996; Gaines & Vorhies, 2016) seen in many examples from outcrop and core (Figs 5 and 10). In such examples, the laminae were observed to have been pushed apart in asymmetrical geometries around the concretion, resulting in a vertically asymmetrical folding of laminae associated with the asymmetrical strain field. Asymmetry is dependent on thick constraining beds, above or below. It is argued, here, that the laminae forcibly fold around concretions by the displacive growth of such asymmetrical concretions (see Fig. 5) in contrast to differential compaction (i.e. symmetrical strain field linked to symmetrical folding patterns) that occurs around replacive concretions.

At the microscale, displacive concretions (Type II-carb) show semi-fibrous calcite crystals (in the form of micro-spar) arranged in random patterns inside the concretion (Fig. 10A to C). This is consistent with the texture of the London Clay displacive carbonate concretions reported by Huggett (1994) and the displacive zones of the carbonate concretions in the Xiamaling Formation in north China reported by Liu et al. (2019).

In addition to the aforementioned indicators, our study presents new diagnostic indicators of concretion growth (Table 1). An important indicator is the formation of the triangular chert areas at the lateral 'pinch points' of the concretions (Figs 2C, 2D, 3D and S8). Triangular chert areas (pinch points) are present in the core, borehole images and at outcrop (Fig. S8) within the lower MCM. They are interpreted here to have formed at the concretion 'pinch points' during its displacive carbonate growth within the host sediment, taking the shape of triangles in cross-section. The authors interpret these features as the result of the diffuse mobilization of silica from the carbonate-rich areas of the concretion to the lateral pinch points where the stress was reduced, thereby favouring the precipitation of silica.

Another diagnostic indicator is the forced folding of the chert beds around Type II-carb concretions, which supports the argument related to displacive growth. Chert beds have been forcibly folded by the displacive development of concretions, which is controlled by the force of crystallization (Dewers & Ortoleva, 1990; Sellés-Martinez, 1996). This leads to an important question of what has controlled the folding of chert beds around concretions.

The folding, around displacive concretions, reaches its maximum at the apogee of the concretion (see Fig. 5A and B); indicating that the asymmetrical nature of the displacive concretions controls this folding. In such cases, displacive growth is interpreted to have occurred when the host rock was not completely lithified. In Fig. 5A, the thick chert bed above the concretion is not folded, whereas below, a thinner, less compacted chert bed intercalated with a set of marl beds hosts a horizon of small carbonate concretions that are folded concordantly with the concretion geometry. This suggests that the folding of chert beds, around this asymmetrical concretion, follows the growth and geometry of the concretion; similar features are seen in Fig. 5B. As noted above, early lithification of chert is commonly seen in these strata as is further evidenced by associated veins. Silica veins are observed to fan radially in the forcibly folded chert beds around Type II-carb concretions, and their apertures increase towards the

maximum curvature (Fig. S5E and F). These silica veins remained orthogonal to the host beds (Fig. S5B to D), indicating that they formed prior to the folding of the chert beds. They are interpreted to have developed during early diagenesis, presumably when the lithification of the chert beds commenced. This is supported by the flat tips of these fractures (Fig. S5). The concretions are believed to have forcibly folded the fractured, semi-lithified chert beds upward and/or downward (with respect to the concretion centre) through its growth history. Consistently, silica veins in the parts of the same chert beds that preserve their horizontal bedding, remained in their original vertical orientation (Fig. S5B to D). Thus, displacive concretionary concretions create increased volume by deforming their host sediments (Sellés-Martinez, 1996).

Another possibility that may explain our forced folding hypothesis is that the chert was sufficiently stiff to influence the folding around displacive concretions, but not brittle enough to fracture, or that the rate of fold growth was so slow that they acted in a ductile manner (for example, like salt). Examples of auto-brecciated chert showing early differential fracturing/microfaulting of brittle chert laminae within thick chert beds are common in the underlying Amman Silicified Limestone (Powell & Moh'd, 2011). The forced folding, regardless of its driving mechanism, should be distinguished from simple differential compaction processes by the extremely localized strain patterns that show asymmetry in the vertical plane linked to the concretion morphology and growth style.

In summary, the abundance of replacive and displacive concretions in the study succession permitted an integrated analysis of the growth mechanism and characterization of growth mode with respect to their stratigraphical position (Fig. 13). Concretion-associated fracturing, including fracturing occurring inside the concretion body and host rock, is crucial to understanding the growth mode of concretions, and is considered an important indicator of displacive growth of concretions (Saigal & Walton, 1988; Sellés-Martinez, 1996).

The fracturing associated with carbonate and chert beds and concretions (including fractures cross-cutting concretions) suggests that: (i) mechanical properties of the strata began to differentiate at a very early stage of burial (Hooker et al., 2017; Abu-Mahfouz et al., 2019), so that type of concretion is dependent on the lithological heterogeneity/homogeneity of the original

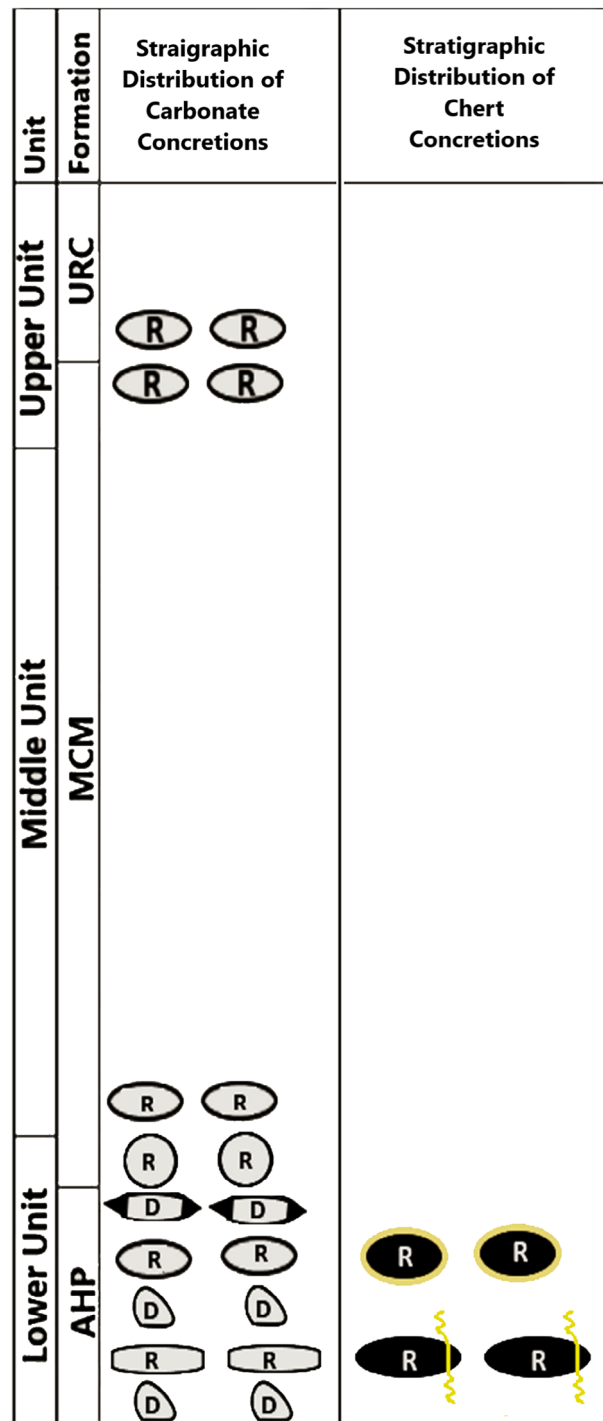**Fig. 13.** Stratigraphical distribution of the different types/morphologies of displacive (D) and replacive (R) carbonate and chert (black) concretions in the study succession. Note the two types of replacive chert concretions: (i) replacive chert concretion cross-cut by early folded calcite veins (wiggly yellow line); and (ii) replacive chert concretion with reaction rims around the concretion (yellow circle).
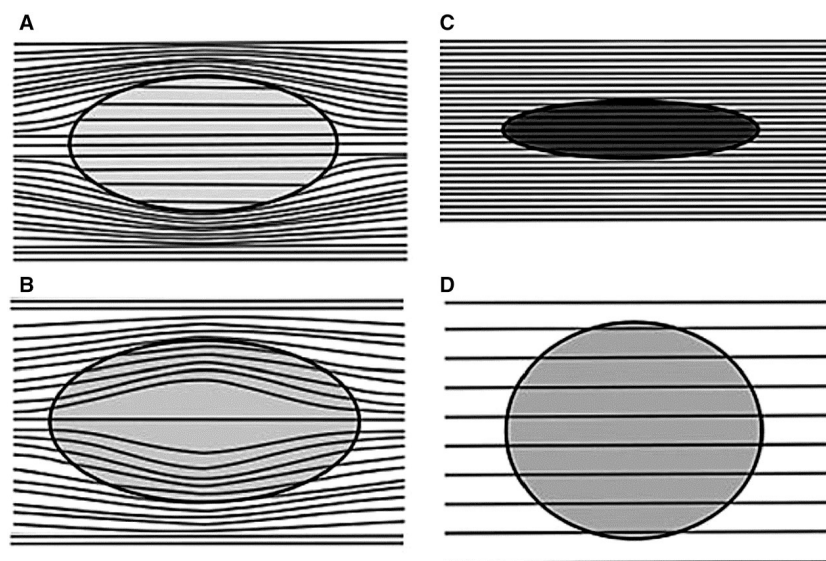
Fig. 14. Diagram showing the different possible occurrences of replacive concretions and their relationships to the host sediment that illustrates the timing of concretion growth relative to sediment compaction. Ellipses represent the outer margin of the concretions. (A) Early diagenetic concretion formed before compaction. (B) Early diagenetic concretion continued to grow during compaction. Note that the beds are deformed inside and outside the concretion; (C) and (D) represent concretions that formed after compaction. Modified from Marshall & Pirrie (2013).

host sediment; and (ii) there is a strong relationship between diagenesis and deformation (Huggett *et al.*, 2017; Abu-Mahfouz *et al.*, 2020).

Timing of concretion growth

The relative timing of the concretion growth can be inferred by analysis of the degree of compaction in the concretion compared with the adjacent host rocks (Astin & Scotchman, 1988; Marshall & Pirrie, 2013; Fig. 14), stable isotope signatures and the growth rate of crystals (Woo & Khim, 2006). Various studies have reported the formation of carbonate concretions at shallow burial depths with different growth rates (e.g. Abed *et al.*, 2005; Makhlouf & El-Haddad, 2006; Huggett *et al.*, 2017; Yoshida *et al.*, 2018). The present study demonstrates that the JOS carbonate concretions (replacive and displacive) formed rapidly during early diagenesis at shallow burial depths but continued to grow during burial history with a relatively slow growth rate (Fig. 15). Evidence for this comes from the following key findings:

At the microscale, the preservation of complete fossils within the carbonate concretions indicates that the concretions formed soon after the deposition of the host sediments (Marshall & Pirrie, 2013; Gao *et al.*, 2020). Fully-preserved fossils and primary depositional structures observed in replacive carbonate concretions (see Fig. 6A) are robust indicators that rapid growth by pore-filling microcrystalline cement occurred prior to burial compaction (Huggett *et al.*, 2000; Raiswell & Fisher, 2000).

The high percentage cement fraction (70 to 80% of pore space is now filled by cement) in both displacive and replacive carbonate concretions implies that cementation occurred at an early stage in the compaction/burial history, where there was sufficient pore space between the primary grains to allow the cement to occupy a large volume of the concretion (Fig. 9; Marshall & Pirrie, 2013). Evidence for rapid growth also includes the presence of only a single cement texture comprised of microcrystalline calcite that is present throughout the carbonate concretion matrix.

The size of the crystals forming the concretions can help to unravel the growth history with regard to the growth rate of concretion (Woo & Khim, 2006). In the case of the JOS carbonate concretions, the increase in the calcite crystal size at the concretion margins of the systematically sampled replacive and displacive concretions may reflect a decrease in the growth rate during the later stages of concretion growth or a reduced strain at the concretion margins permitting larger crystal growth.
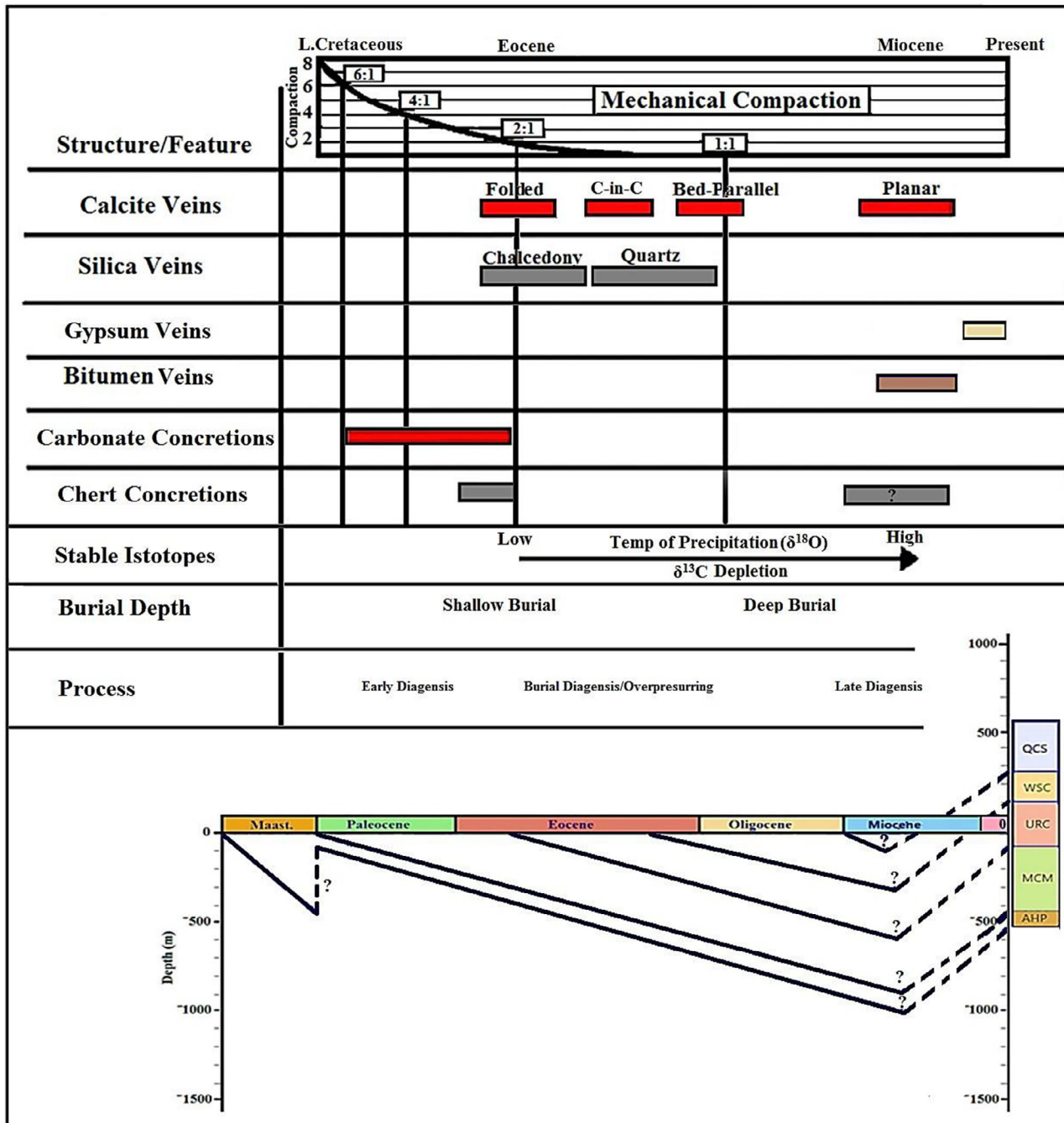
Fig. 15. Paragenetic sequence of concretion formation and cement of the associated fracture sets. The timing of the different features is relatively constrained based on cross-cutting relationships (between fractures and concretions), compaction ratio/burial history and stable isotopes analyses. AHP, Al-Hisa Phosphorite Formation; MCM, Muwaqqer Chalk-Marl Formation; QCS, Qirma Sandstone Formation; URC, Umm Rijam Chert-Limestone Formation; WSC, Wadi Shallalah Chalk Formation.

Geochemically, the narrow ranges of the stable isotopic values of the systematically analysed carbonate concretions ($\delta^{13}C$ compositions range from −7.13 to −6.07‰ for replacive concretions and from −10.58 to −8.15‰ for displacive concretions; and $\delta^{18}O$ values range from −9.35 to −4.38‰ for both concretion types) and their host rocks ($\delta^{13}C$ values range from −9.40 to

−7.17‰) (Table 2; Fig. 11) suggest an early formation of concretions at shallow depths. This narrow range suggests that pore water chemistry remained similar during growth and that the concretion growth over time did not occur rapidly. The $\delta^{13}C$ values of carbonates that form the concretion matrix are usually used to characterize specific microbial pathways that were responsible for commencing and maintaining concretion growth, and constrain the timing and duration of growth (Coleman & Raiswell, 1981, 1995; Mozley & Burns, 1993; Fisher et al., 1998; Raiswell & Fisher, 2000, 2004; Raiswell et al., 2002; Dale et al., 2014; Loyd et al., 2014). The narrow isotopic ranges, along with the finding that the concretion margins are usually more depleted than the centres (isotopic values of the centres are close to the host-rock values) and the $\delta^{18}O$ isotopic compositions (low temperatures of precipitation) of both Type-1 carb (replacive) and Type II-carb (displacive) concretions suggest that concretion formation commenced at shallow burial depth, but may have continued during progressive burial (Raiswell, 1971; De Craen et al., 1998; Raiswell & Fisher, 2000; Woo & Khim, 2006; Marshall & Pirrie, 2013; Gaines & Vorhies, 2016). The $\delta^{18}O$ ratios (−9.35 to −4.38‰) indicate that the precipitation occurred not far below the sediment–water interface, mostly from CO_2 produced by sulphate-reducing bacteria (Irwin et al., 1977).

Different relationships between concretions and their associated fractures also help to constrain the timing of concretion growth. The presence of septarian fractures inside the Type II-carb concretions (MCM) strongly indicates an early formation of these concretions (Fig. 7A; Raiswell, 1971; Astin, 1986; Astin & Scotchman, 1988; Hesslebo & Palmer, 1992; Marshall & Pirrie, 2013; Gao et al., 2020). Septarian fractures have been reported in many mudstone-dominated successions such as the Lias Group (Lower Jurassic) and Kimmeridge Clay Formation (Upper Jurassic) in Dorset, UK (e.g. Hesslebo & Palmer, 1992; Wolff et al., 1992; Kiriakoulakis et al., 2000). Hesslebo & Palmer (1992) argued that septarian cracks formed within concretions probably during the early stages of burial at burial depths of no greater than 30 m. Some authors have characterized septarian fractures as tensile fractures that usually form during the burial and compaction of the host sediments (Astin, 1986; Maltman, 1994; Sellés-Martinez, 1996; Hounslow, 1997). Astin (1986) argued that they are tensile fractures that form by dehydration during diagenesis.

Hounslow (1997) suggested that they might form over a wide depth range. However, Hounslow (1997) suggests that a condition for their formation is that the pore pressure is higher inside the concretion than in the host sediment, thereby generating local overpressuring that led to internal fracturing. It was suggested that this may have occurred because early cementation reduced the permeability of the concretion, confining the fluids in the concretion. Sellés-Martinez (1996) proposed that it is possible for septarian cracks to develop due to the increase of stress around a stiff concretion in plastic sediment, suggesting that overpressuring is not essential for septarian fracturing (Raiswell & Fisher, 2000). Wetzel (1992) noted that septarian fracture formation may be initiated by both plastic deformation and dewatering of the concretion body.

The radial orientation of silica veins in the thin chert beds around displacive carbonate concretions (Fig. 5A) implies that growth of the carbonate concretion post-dates early fracturing of the chert and subsequent infilling by silica, the latter thought to be coeval with the folding of the chert beds. Radial fanning of silica veins is usually associated with an increase in the aperture size of silica veins (up to 3 cm width) at the areas of maximum curvature (Fig. S5C to F), providing robust evidence of the early formation of these Type II-carb concretions. The progressive concretion growth appears to have contributed to the increase of the vein aperture and silica fill; early fracturing is also supported by the orthogonal direction of similar veins in the adjacent level-bedded chert (Fig. S5B to D).

Vertical planar calcite veins, in contrast, were observed in many examples to cross-cut the carbonate concretions and the surrounding beds (Fig. S5C and D), indicating that these veins post-date the growth of the concretions. This is supported by the stable isotopic data that show that cross-cutting calcite veins are more depleted in carbon and show the most negative $\delta^{18}O$ signatures compared to concretions and the host sediments.

The bending of a horizon of small carbonate concretions around a displacive carbonate concretion in the AHP (Fig. 5A) is another piece of evidence that this deformation occurred due to the displacive growth of the main concretion, as indicated by the downward bending that is concordant with the concretion shape and growth. Additionally, joint fractures at the lower boundary of the overlying thick chert bed indicate that the fracturing had occurred in this bed prior to concretion growth, possibly as a result of the
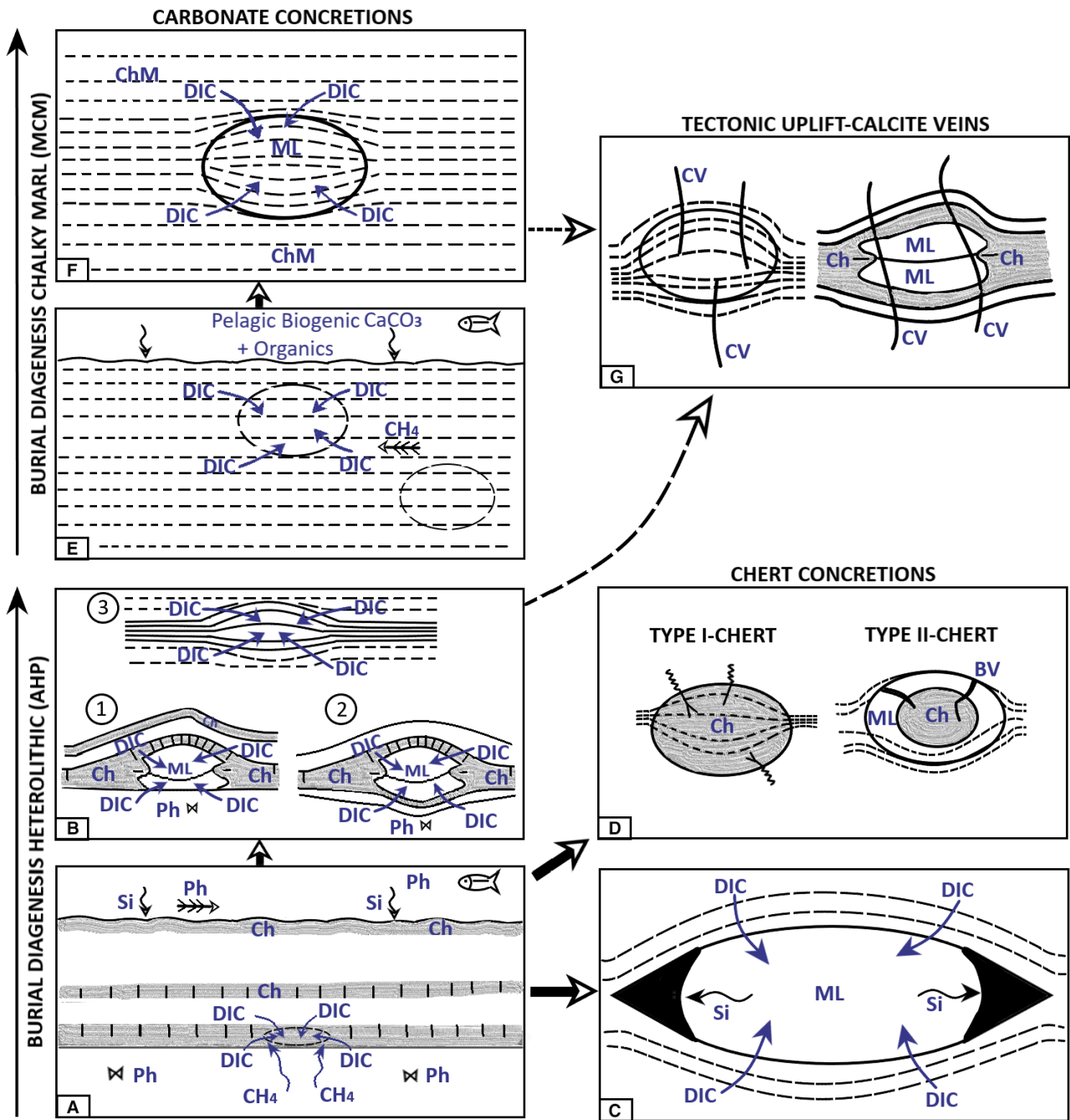
Fig. 16. Schematic drawing illustrating the sequence of diagenetic events (A) to (G) in heterolithic (Al-Hisa Phosphorite Formation – AHP – A to D) and homogeneous (Muwaqqer Chalk-Marl Formation/Umm Rijam Chert-Limestone Formation – MCM/URC – E to F) primary lithologies in the study section. (A) to (D) Deposition of phosphorite, chert (opal-A to opal-CT and siliceous chert transition) in the AHP; the formation of displacive (B1, B2) and replacive (B3) carbonate concretions, early formed silica veins (A), and replacive chert concretions is shown in (B) to (D) at shallow burial depths in the presence of alkaline pore waters with dissolved inorganic carbon (DIC); the formation, at greater burial depths, of folded calcite veins, bitumen veins (BV) and chert 'wings' is shown in (D) and (C), respectively. (E) and (F) Illustrate the deposition of chalky marl (MCM) and chalky marl with chert (URC) with the formation of replacive carbonate concretions. Late-stage tectonic uplift resulted in planar calcite veins cross-cutting concretions and host rocks (G). Ch, chert; CH_4, methane; ChM, chalky marl; CV, late calcite veins; DIC, dissolved inorganic carbon; ML, microcrystalline limestone; Ph, phosphate; Si, silica.

early lithified chert becoming more brittle during shallow burial diagenesis.

Another strong line of evidence on the early timing of concretion growth is the formation of triangular areas that are filled by chert at the lateral margins of some of the displacive carbonate concretions (ear-like shape; Figs 2C, 2D, 3D and S8). These triangular chert spaces indicate the migration of mobilized silica ions to lateral margins of the concretion where the compressional growth pressure was reduced; they are interpreted as forming during later stages of carbonate concretion growth in a semi-closed system with reduced DIC that favoured the migration of silica ions to these marginal regions. The 'chert wings' are distinguished from the 'displacive splitting' of primary chert beds seen in Fig. 5B and C.

Geomechanically, the compaction ratios of replacive carbonate concretions indicate that these concretions formed rapidly in the first few metres, prior to any significant compaction, and continued to grow during burial and compaction (Fig. 15). This is indicated by the enhanced differential compaction of the host mudstone leading to the bending of shale and marl laminae around concretions (Marshall & Pirrie, 2013).

Although the deflection of bedding around the concretions is a primary feature associated with different types of concretions (Raiswell, 1971; Mozley, 1996; Raiswell & Fisher, 2000; Rodrigues *et al.*, 2009), the beds were observed to show a high and an asymmetrical deflection (i.e. asymmetrical strain field) around displacive concretions (Fig. 3B and Fig. S7), which contrast with symmetrical differential compaction around replacive concretions.

The aforementioned interpretation of the early formation of carbonate concretions also applies to Type I-ch concretions. The cross-cutting relationship with the early folded calcite veins (Fig. 2H) is a strong line of evidence that these concretions formed at a very early stage of burial.

Type II-ch concretions (Fig. 2J) are, however, believed to have formed relatively later (Fig. 15), and their formation (silica diagenesis) has promoted hydrocarbon expulsion resulting in bitumen fractures that later cross-cut these concretions (Abu-Mahfouz *et al.*, 2020). In addition, no evidence of cross-cutting by folded calcite veins was observed in this type of concretion.

To summarize, Fig. 16 shows the sequence of events (through time) from the deposition of the host rocks [carbonates, organic matter and chert sols (opal CT-chert transition)], through the formation of folded calcite veins, silica veins, concretion development, development of reaction rims around chert concretions, and late calcite veins.

CONCLUSIONS

1 This study makes a new contribution to the understanding of the growth modes of concretions in organic-rich, heterolithic phosphorites and bituminous carbonate mudrocks.

2 Carbonate and chert concretions are abundant in the upper and lower intervals of the upper Maastrichtian to Eocene study succession in central Jordan. Specific concretion types and compositions typically occur in specific stratigraphic horizons, their structure and mode of development largely controlled by the lithological nature of the original host sediment (rock), that is cherty phosphorite versus bituminous chalky mudrock.

3 Two main modes of growth were observed in these rocks: (i) displacive concretion growth; and (ii) replacive concretion growth.

4 This study presents new evidence for displacive concretion growth based on: (i) asymmetrical folding (due to displacive growth pressure) associated with the asymmetrical strain field around concretions, and silica vein arrays; (ii) the formation of triangular chert areas at the margins of carbonate concretions; and (iii) the semi-fibrous nature of calcite crystals forming these concretions.

5 Based on macroscopic and microscopic evidence and stable isotope results, concretion formation is interpreted as commencing at shallow burial depth in the presence of alkaline pore waters with abundant Mg^{2+} ions. The presence of available organic matter (from phytoplankton and fish/vertebrate clasts) and redox-sensitive metals such as U and Mo derived mainly from phosphate and organic matter may have favoured concretion genesis through migration of pore waters rich in dissolved organic carbon. Growth continued during progressive burial for Type I-carbonate concretions.

6 Displacive Type II-carbonate concretions in the AHP are interpreted to have formed in a semi-closed system, locally confined by thick, mechanically stronger, beds of chert or phosphate. In contrast, replacive Type I carbonate concretions are thought to have developed more slowly in homogeneous chalky marl (locally bituminous) sediments.

7 Chert concretions are interpreted to have different timing of development: early for

replace Type I-chert concretions with folded calcite veins and late for Type II-chert concretions with halo/reaction rims and bitumen veins.

ACKNOWLEDGEMENTS

We acknowledge Shell PLC represented by the Jordan Oil Shale Company (JOSCO) for providing the core samples for this study. The editor (Kevin Taylor) and reviewers (Joe Emmings and the anonymous reviewer) are sincerely thanked for the thorough and constructive comments on our original manuscript.

DATA AVAILABILITY STATEMENT

All data are available upon request.

REFERENCES

Abed, A.M., **Arouri, K.R.** and **Boreham, C.J.** (2005) Source rock potential of the phosphorite– bituminous chalk–marl sequence in Jordan. *Mar. Petrol. Geol.*, **22**, 413–425.

Abu-Jaber, N., **Kimberley, M.** and **Cavaroc, V.** (1989) Mesozoic-Paleogene basin development within the eastern Mediterranean borderland. *J. Petrol. Geol.*, **12**, 419–436.

Abu-Mahfouz, I.S. (2019) Genesis of natural fracture systems in Mudrocks (Upper Cretaceous-Eocene), Jordan. PhD Thesis, University of Oxford. 409 pp.

Abu-Mahfouz, I.S., **Cartwright, J.**, **Idiz, E.**, **Hooker, J.**, **Robinson, S.** and **Boorn, S.** (2019) Genesis and role of bitumen in fracture development during early catagenesis. *Petrol. Geosci.*, **25**, 371–388.

Abu-Mahfouz, I.S., **Cartwright, J.**, **Idiz, E.**, **Hooker, J.N.** and **Robinson, S.** (2020) Silica diagenesis promotes early primary hydrocarbon migration. *Geology*, **48**, 483–487.

Abu-Mahfouz, I.S., **Gaus, G.**, **Grohmann, S.**, **Klaver, J.**, **Cartwright, J.**, **Idiz, E.**, **Littke, R.**, **Urai, J.L.**, **Patzek, T.** and **Vahrenkamp, V.** (2022a) Improved understanding of hydrocarbon expulsion and associated fracturing during successive stages of maturation: insights from the artificial maturation of organic-rich, immature to early mature source rocks. Presented at the 2022 International Petroleum Technology Conference, Riyadh International Convention and Exhibition Centre in Riyadh, Kingdom of Saudi Arabia, 12 pp.

Abu-Mahfouz, I.S., **Wicaksono, A.N.**, **Idiz, E.**, **Cartwright, J.**, **Santamarina, C.J.** and **Vahrenkamp, V.** (2022b) Modelling the initiation of bitumen-filled microfractures in immature, organic-rich carbonate mudrocks: the Maastrichtian source rocks of Jordan. *Mar. Pet. Geol.*, **141**, 105700.

Abu-Mahfouz, I.S., **Iakusheva, R.**, **Finkbeiner, T.**, **Cartwright, J.** and **Vahrenkamp, V.** (2023) Rock mechanical properties of immature, organic-rich source rocks and their relationships to rock composition and lithofacies. *Petrol. Geosci.* https://doi.org/10.1144/petgeo2022-021.

Alqudah, M., **Ali Hussein, M.**, **Podlaha, O.G.**, **van den Boorn, S.** and **Mutterlose, J.** (2015) Biostratigraphy and depositional setting of Maastrichtian – Eocene oil shales from Jordan. *Mar. Pet. Geol.*, **60**, 87–104.

Astin, T.R. (1986) Septarian crack formation in carbonate concretions from shales and mudstones. *Clay Miner.*, **21**, 617–631.

Astin, T.R. and **Scotchman, I.C.** (1988) The diagenetic history of some septarian concretions from the Kimmeridge clay, England. *Sedimentology*, **35**, 349–368.

Behl, R.J. and **Garrison, R.E.** (1994) The origin of chert in the Monterey Formation of California (USA). In: *Siliceous, Phosphatic and Glauconitic Sediments of the Tertiary and Mesozoic: 29th International Geological Congress, Proceedings, Part C* (Eds Iijima, A., Abed, A. and Garrison, R.), pp. 101–132. VSP, Utrecht.

Bisque, R. (1962) Clay polymerisation in carbonate rocks: silicification reaction defined. Abstract, Ninth National Conference on Clays and Clay Minerals, 123 pp.

Bohrmann, G., **Abelmann, A.**, **Gersonde, R.**, **Hubberten, H.** and **Kuhn, G.** (1994) Pure siliceous ooze, a diagenetic environment for early chert formation. *Geology*, **22**, 207–210.

Chan, M.A., **Ormö, J.**, **Park, A.J.**, **Stich, M.**, **Souza-Egipsy, V.** and **Komatsu, G.** (2007) Models of iron oxide concretion formation: field, numerical, and laboratory comparisons. *Geofluids*, **7**, 356–368.

Coleman, M. and **Raiswell, R.** (1981) Carbon, oxygen and Sulphur isotope variations in concretions from the upper Lias of NE England. *Geochim. Cosmochim. Acta*, **45**, 329–340.

Coleman, M.L. and **Raiswell, R.** (1995) Source of carbonate and origin of zonation in pyritiferous carbonate concretions; evaluation of a dynamic model. *Am. J. Sci.*, **295**, 282–308.

Craig, J. (1985) Tectonic evolution of the area between Borth and Cardigan, Dyfed, West Wales. Unpublished PhD Thesis, University College of Wales, Aberystwyth.

Dale, A., **John, C.M.**, **Mozley, P.S.**, **Smalley, P.C.** and **Muggeridge, A.H.** (2014) Time-capsule concretions: unlocking burial diagenetic processes in the Mancos shale using carbonate clumped isotopes. *Earth Planet. Sci. Lett.*, **394**, 30–37.

Davies, R.J. (2005) Differential compaction and subsidence in sedimentary basins due to silica diagenesis: a case study. *Geol. Soc. Am. Bull.*, **117**, 1146–1155.

Davies, R.J., **Cartwright, J.A.** and **Rana, J.** (1999) Giant hummocks in deep-water marine sediments: evidence for large-scale differential compaction and density inversion during early burial. *Geology*, **27**, 907–910.

De Craen, M., **Swennen, R.** and **Keppens, E.** (1998) Petrography and geochemistry of septarian carbonate concretions from the boom clay formation (Oligocene, Belgium). *Geol. Mijnbouw*, **77**, 63–76.

Dewers, T. and **Ortoleva, P.** (1990) Force of scrystallisation during the growth of siliceous concretions. *Geology*, **18**, 204–207.

Dix, G.R. and **Mullins, H.T.** (1987) Shallow, subsurface growth and burial alteration of middle Devonian calcite concretions. *J. Sediment. Res.*, **57**, 140–152.

Eichhubl, P. and **Behl, R.J.** (1998) *Diagenesis, deformation, and fluid flow in the Miocene Monterey Formation*. Pacific Section, SPEM Specical Publication, Book, 98 pp.

Emmings, J.F., **Davies, S.J.**, **Vane, C.H.**, **Moss-Hayes, V.** and **Stephenson, M.H.** (2020) From marine bands to hybrid

flows: sedimentology of a Mississippian black shale. *Sedimentology*, **67**, 261–304.

Feinstein, S., **Eyal, M.**, **Kohn, B.**, **Steckler, M.**, **Ibrahim, K.**, **Moh'd, B.** and **Tian, Y.** (2013) Uplift and denudation history of the eastern Dead Sea rift flank, SW Jordan: evidence from apatite fission track thermochronometry. *Tectonics*, **32**, 1513–1528.

Fisher, Q., **Raiswell, R.** and **Marshall, J.** (1998) Siderite concretions from nonmarine shales (Westphalian a) of the Pennines, England: controls on their growth and composition. *J. Sed. Res.*, **68**, 1034–1045.

Fossen, H. (2016) *Structural Geology*. Cambridge University Press, Cambridge.

Gaines, R.R. and **Vorhies, J.S.** (2016) Growth mechanisms and geochemistry of carbonate concretions from the Cambrian wheeler formation (Utah, USA). *Sedimentology*, **63**, 662–698.

Gao, P., **He, Z.**, **Lash, G.**, **Li, S.** and **Zhang, R.** (2020) Origin of chert nodules in the Ediacaran Doushantuo formation black shales from Yangtze block, South China. *Mar. Petrol. Geol.*, **114**, 104227.

Garrison, R.E. (1981) Diagenesis of oceanic carbonate sediments: a review of the DSDP perspective. *SEPM Spec. Publ.*, **32**, 181–207.

Grohmann, S., **Gaus, G.**, **Klaver, J.**, **Abu Mahfouz, I.S.**, **Vahrenkamp, V.**, **Patzek, T.**, **Urai, J.** and **Littke, R.** (2021) *Hydrous Pyrolysis of Source Rock Plugs: Geochemical and Visual Investigations and Implications for Primary Migration*. European Association of Geoscientists & Engineers, Houten, The Netherlands.

Grohmann, S., **Littke, R.**, **Abu-Mahfouz, I.S.**, **Gaus, G.**, **Klaver, J.**, **Thüns, N.**, **Schulte, P.**, **Patzek, T.** and **Vahrenkamp, V.** (2023) The deposition of type II-S Jordan oil shale in the context of Late Cretaceous source rock formation in the Eastern Mediterranean realm. Insights from organic and inorganic geochemistry and petrography. *Mar. Petrol. Geol.*, **148**, 106058.

Hakimi, M.H., **Abdullah, W.H.**, **Alqudah, M.**, **Makeen, Y.M.** and **Mustapha, K.A.** (2016) Organic geochemical and petrographic characteristics of the oil shales in the Lajjun area, Central Jordan: origin of organic matter input and preservation conditions. *Fuel*, **181**, 34–45.

Hesse, R. and **Schacht, U.** (2011) Early diagenesis of deep-sea sediments. In: *Developments in Sedimentology*, Vol. 63 (Eds HüNeke, H. and Mulder, T.), pp. 557–713. Elsevier, Amsterdam, The Netherland.

Hesslebo, S.P. and **Palmer, T.J.** (1992) Reworked early diagenetic concretions and the bioerosional origin of a regional discontinuity within British Jurassic marine mudstones. *Sedimentology*, **39**, 1045–1065.

Hooker, J.N., **Huggett, J.M.**, **Cartwright, J.A.** and **Ali Hussein, M.** (2017) Regional-scale development of opening-mode calcite veins due to silica diagenesis. *Geochem. Geophys. Geosyst.*, **18**, 2580–2600.

Hooker, J.N., **Abu-Mahfouz, I.S.**, **Meng, Q.** and **Cartwright, J.** (2019) Fractures in mudrocks. Advances in constraining timing and understanding mechanisms. *J. Struct. Geol.*, **125**, 166–173.

Hounslow, M.W. (1997) Significance of localized pore pressure to the genesis of septarian concretions. *Sedimentology*, **44**, 1133–1147.

Huggett, J.M. (1994) Diagenesis of mudrocks and concretions from the London clay formation in the London Basin. *Clay Miner.*, **29**, 693–707.

Huggett, J.M., **Gale, A.S.** and **Evans, S.** (2000) Carbonate concretions from the London clay (Ypresian, Eocene) of southern England and the exceptional preservation of wood-boring communities. *J. Geol. Soc. London*, **157**, 187–200.

Huggett, J., **Hooker, J.N.** and **Cartwright, J.A.** (2017) Lithologic controls on diagenesis and diagenetic sequence in the Al Hasa phosphorite, Muwaqqar chalk marl, and um Rijam chert formations, Jordan, Arabian. *J. Geosci.*, **10**, 270.

Irwin, H., **Curtis, C.** and **Coleman, M.** (1977) Isotopic evidence for source of diagenetic carbonates formed during burial of organic-rich sediments. *Nature*, **269**, 209–213.

Isaacs, C.M. (1982) Influence of rock composition on kinetics of silica phase changes in the Monterey Formation, Santa Barbara area, California. *Geology*, **10**, 304–308.

Kastner, M., **Keene, J.B.** and **Gieskes, J.M.** (1977) Diagenesis of siliceous oozes. 1. Chemical controls on the rate of opal-a to opal-CT transformation – an experimental study Geochim. Cosmochim. *Acta Theriol.*, **41**, 1041–1059.

Kiriakoulakis, K., **Marshall, J.D.** and **Wolff, G.A.** (2000) Biomarkers in a lower Jurassic concretion from Dorset (UK). *J. Geol. Soc. London*, **157**, 207–220.

Kolodny, Y. (1969) Petrology of the siliceous rocks in the Mishash formation (Negev, Israel). *J. Sediment. Petrol.*, **39**, 165–175.

Kolodny, Y., **Taraboulos, A.** and **Frieslander, U.** (1980) Participation of fresh water in chert diagenesis: evidence from oxygen isotopes and boron α-track mapping. *Sedimentology*, **27**, 305–316.

Lash, G.G. and **Blood, D.R.** (2004) Depositional clay fabric preserved in early diagenetic carbonate concretion pressure shadows, upper Devonian (Frasnian) Rhinestreet shale, western NewYork. *J. Sediment. Res.*, **74**, 110–116.

Lash, G.G. and **Blood, D.R.** (2007) Origin of early overpressure in the upper Devonian Catskill Delta complex, western New York state. *Basin Res.*, **19**, 51–66.

Liu, A.-Q., **Tang, D.-J.**, **Shi, X.-Y.**, **Zhou, L.-M.**, **Zhou, X.-Q.**, **Shang, M.-H.**, **Li, Y.** and **Song, H.-Y.** (2019) Growth mechanisms and environmental implications of carbonate concretions from the ~ 1.4 Ga Xiamaling formation, North China. *J. Paleogeog.*, **8**, 20.

Loyd, S.J., **Dickson, J.**, **Boles, J.R.** and **Tripati, A.K.** (2014) Clumped-isotope constraints on cement paragenesis in septarian concretions. *J. Sed. Res.*, **84**, 1170–1184.

Makhlouf, I.M. and **El-Haddad, A.A.** (2006) Depositional environments and facies of the late Triassic Abu Ruweis formation, Jordan. *J. Asian Earth Sci.*, **28**, 372–384.

Maliva, R.G. and **Siever, R.** (1988) Diagenetic replacement controlled by force of crystallization. *Geology*, **16**, 688–691.

Maltman, A. (1994) Introduction and overview. In: *The Geological Deformation of Sediments* (Ed Maltman, A.), p. 1±35. Chapman & Hall, London.

Marshall, J.D. and **Pirrie, D.** (2013) Carbonate concretions— explained. *Geol. Today*, **29**, 53–62.

März, C., **Wagner, T.**, **Aqleh, S.**, **al-Alaween, M.**, **van den Boorn, S.**, **Podlaha, O.G.**, **Kolonic, S.**, **Poulton, S.W.**, **Schnetger, B.** and **Brumsack, H.J.** (2016) Repeated enrichment of trace metals and organic carbon on an Eocene high-energy shelf caused by anoxia and reworking. *Geology*, **44**, 1011–1014.

Meng, Q., **Hooker, J.N.** and **Cartwright, J.** (2018) Lithological control on fracture cementation in the Keuper marl (Triassic), North Somerset, UK. *Geol. Mag.*, **155**, 1761–1775.

Moshkovitz, S., **Erlich, A.** and **Soudry, D.** (1983) Siliceous microfossils of the Upper Cretaceous Mishash Formation, central Negev, Israel. *Cretaceous Res.*, **4**, 73–194.

Mozley, P.S. (1996) The internal structure of carbonate concretions in mudrocks: a critical evaluation of the conventional concentric model of concretion growth. *Sed. Geol.*, **103**, 85–91.

Mozley, P.S. and **Burns, S.J.** (1993) Oxygen and carbon isotopic composition of marine carbonate concretions: an overview. *J. Sed. Res.*, **63**, 73–83.

Murray, R.W., **Jones, D.L.** and **Brink, M.R.B.T.** (1992) Diagenetic formation of bedded chert: evidence from chemistry of the chert-shale couplet. *Geology*, **20**, 271–274.

Nelson, C.S. and **Lawrence, M.F.** (1984) Methane-derived high-Mg calcite submarine cement in Holocene nodules from the Fraser Delta, British Columbia, Canada. *Sedimentology*, **31**, 645–654.

Pearson, M. and **Nelson, C.** (2005) Organic geochemistry and stable isotope composition of New Zealand carbonate concretions and calcite fracture fills. *NZ J. Geol. Geophys.*, **48**, 395–414.

Powell, J.H. (1989) Stratigraphy and sedimentation of the Phanerozoic rocks in central and south Jordan. Natural Resources Authority, Geological Mapping Division, Bulletin 11 Part B, Kurnub, Ajlun and Belqa groups, {part A was Lower Palaeozoic}, Amman, 130 pp.

Powell, J.H. and **Moh'd, B.K.** (2011) Evolution of cretaceous to Eocene alluvial and carbonate platform sequences in central and South Jordan. *GeoArabia*, **16**, 29–82.

Powell, J.H. and **Moh'd, B.K.** (2012) Early diagenesis of late cretaceous chalk-chert-phosphorite hardgrounds in Jordan: implications for sedimentation on a Coniacian-Campanian pelagic ramp. *GeoArabia*, **17**, 17–38.

Raiswell, R. (1971) The growth of Cambrian and Liassic concretions. *Sedimentology*, **17**, 147–171.

Raiswell, R. (1976) The microbiological formation of carbonate concretions in the upper Lias of NE England. *Chem. Geol.*, **18**, 227–244.

Raiswell, R. (1988) Evidence for surface reaction-controlled growth of carbonate concretions in shales. *Sedimentology*, **35**, 571–575.

Raiswell, R. and **Fisher, Q.J.** (2000) Mudrock-hosted carbonate concretions: a review of growth mechanisms and their influence on chemical and isotopic composition. *J. Geol. Soc. London*, **157**, 239–251.

Raiswell, R. and **Fisher, Q.** (2004) Rates of carbonate cementation associated with sulphate reduction in DSDP/ODP sediments: implications for the formation of concretions. *Chem. Geol.*, **211**, 71–85.

Raiswell, R., **Bottrell, S.H.**, **Dean, S.P.**, **Marshall, J.D.**, **Carr, A.** and **Hatfield, D.** (2002) Isotopic constraints on growth conditions of multiphase calcite-pyrite-barite concretions in carboniferous mudstones. *Sedimentology*, **4**, 237–254.

Richardson, W.A. (1921) The relative age of concretions. *Geol. Mag.*, **63**, 114–124.

Rodrigues, N., **Cobbold, P.R.**, **Loseth, H.** and **Ruffet, G.** (2009) Widespread bedding-parallel veins of fibrous calcite ('beef') in a mature source rock (Vaca Muerta Fm, Neuquén Basin, Argentina): evidence for overpressure and horizontal compression. *J. Geol. Soc. London*, **166**, 695–709.

Saigal, G.C. and **Walton, E.K.** (1988) On the occurrence of displacive calcite in lower old red sandstone of Carnoustie, eastern Scotland. *J. Sediment. Res.*, **58**, 131–135.

Sellés-Martinez, J. (1996) Concretion morphology, classification and genesis. *Earth Sci. Rev.*, **41**, 177–210.

Shawabkeh, K. (1991) The Geology of Adir area, Map Sheet No. 3152-II. Nat. Res. Auth., Geol. Dir., Geol. Map. Div., Bulletin, 18, 31 pp, Amman.

Sheikholeslami, R., **Al-Mutazb, I.S.**, **Tan, S.** and **Tan, S.D.** (2002) Some aspects of silica polymerization and fouling and its pretreatment by sodium aluminate, lime and soda ash. *Desalination*, **150**, 85–92.

Soudry, D. and **Champetier, Y.** (1983) Microbial processes in the Negev phosphorites (southern Israel). *Sedimentology*, **30**, 411–423.

Torres, M.E., **Hong, W.L.**, **Solomon, E.A.**, **Milliken, K.**, **Kim, J.H.**, **Sample, J.C.**, **Teichert, B.M.** and **Wallmann, K.** (2020) Silicate weathering in anoxic marine sediment as a requirement for authigenic carbonate burial. *Earth-Sci. Rev.*, **200**, 102960.

Varela, D.E., **Willers, V.** and **Crawford, D.W.** (2011) Effect of zinc availability on growth, morphology and nutrient incorporation in a coastal and an oceanic diatom. *J. Phycol.*, **47**, 302–312.

Wetzel, A. (1992) An apparent concretionary paradox. Zbl.Geol. Pala. Èontol., Teil1 (1991), 2823±2830.

Wolff, G.A., **Rukin, N.** and **Marshall, J.D.** (1992) Geochemistry of an early diagenetic concretion from the Birchi bed (L. Lias, W. Dorset, UK). *Org. Geochem.*, **19**, 431–444.

Woo, K.S. and **Khim, B.K.** (2006) Stable oxygen and carbon isotopes of carbonate concretions of the Miocene Yeonil Group in the Pohang Basin, Korea: types of concretions and formation condition. *Sed. Geol.*, **183**, 15–30.

Xiao, S., **Schiffbauer, J.D.**, **McFadden, K.A.** and **Hunter, J.** (2010) Petrographic and SIMS pyrite sulfur isotope analyses of Ediacaran chert nodules: implications for microbial processes in pyrite rim formation, silicification, and exceptional fossil preservation. *Earth Planet. Sci. Lett.*, **297**, 481–495.

Yoshida, H., **Yamamoto, K.**, **Minami, M.**, **Katsuta, N.**, **Sin-ichi, S.** and **Metcalfe, R.** (2018) Generalised conditions of spherical carbonate concretion formation around decaying organic matter in early diagenesis. *Sci. Rep.*, **8**, 6308.

Supporting Information

Additional information may be found in the online version of this article:

Figure S1. (A) Field photograph showing the AHP, MCM and URC formations exposed at Wadi Al-Bustani, south Jordan. Height of section *ca* 60 m. (B) Field photograph showing the concretions on a bedding plane in Wadi AL-Bustani (hammer circled for scale).

Figure S2. Example of fractures and concretions from the borehole images. CC, Carbonate Concretion; Ch, Chert.

Figure S3. BSE image of replacive carbonate concretion from the MCM, Core C9.

Figure S4. Histogram showing the diameter values (the longer axis in spherical concretions) of carbonate and chert concretions in all the study outcrops.

Figure S5. (A) Field photograph showing folding of chert beds around a horizon of carbonate concretions in the Qatrana Roadcut (AHP). (B) Field photograph showing silica veins orthogonal to the chert beds bending around the concretion. (C) Zoom-in of the red square in (A) showing an asymmetrical carbonate concretion with a folding of the chert bed underlying the concretion. (D) Drawing of (C), showing silica veins (white lines) confined to the chert bed bending around the concretion and planar calcite veins (red lines) that crosscut the carbonate concretion and the host beds. SV, Silica Vein; CV, Calcite Vein. Note the maximum aperture size in the areas that show a high degree of folding. (E) Frequency distribution of the fracture aperture of silica veins observed in the chert beds around carbonate concretions in the area with maximum folding (areas of localized deformation). (F) Frequency distribution of the fracture aperture of silica veins in the non-folded/undeformed parts (i.e. away from the concretion) of the same host (chert) beds.

Figure S6. Bedding-parallel gypsum veins transecting a carbonate concretion.

Figure S7. Microphotograph in polarized light showing a chalcedony-filled radiolarian test.

Figure S8. Examples from the core (A), borehole image logs (B) and outcrop (C) of triangular spaces formed at the pinch points at the margins of the carbonate concretions. Ch: Chert; CC, Carbonate Concretion; S. Lst, Silicified Limestone.

Table S1. Table summarizes the locations and key information about the study outcrops.